Frequency Resolved Optical Gating measurements on a stretched Mid-IR laser source

Master's thesis
by
Martin Haag

Lund Reports on Atomic Physics, LRAP-388
ETH Zurich, August 2007
Institute of Quatum Electronics

Eidgenössische Technische Hochschule Zürich
Swiss Federal Institute of Technology Zurich

LUNDS UNIVERSITET
Lunds Tekniska Högskola

Abstract

A laser with pulse energies of 1 μJ at 3.6 μm and with a repetition rate of 100 kHz with a spectrum supporting pulses down to 50 to 100 fs is a promising source of laser radiation for use in high field physics and attosecond science. In order to be used in experiments, the laser needs to be fully characterized.

We report on a frequency resolved optical gating (FROG) setup capable of measuring on two different frequencies, 1.07 and 3.6 μm. The FROG setup uses second harmonic generation (SHG). Measurements showed that a prism situated in the seed laser for the mid-infrared radiation needs to be moved to obtain minimal group delay dispersion (GDD) on the seed laser. At the current optimal position, there exists a residual GDD of 1000 fs^2.

During the measurements on the mid-infrared laser, severe instabilities on the laser were noticed. This limits the accuracy of the measurements made. It was concluded that, before any use in experiments could be made, the laser needed to be stabilized. The currently stretched laser pulse at 3.6 μm was determined to have a temporal full width half maximum (FWHM) of 2.3 ps, a spectral FWHM of 200 nm and a GDD of 100000 fs^2.

Summary

High order harmonics generation (HHG) is a commonly used method for creating extreme ultraviolet laser pulses. Atoms positioned in a strong laser field respond in a nonlinear way, emitting high order harmonics. The cut off energy of the harmonics limits the pulse duration of the generated laser pulses. To increase the cut off energy one can either increase the power of the laser up to a certain point or go to higher wavelengths. The cut off energy scales linearly with the power and with the square of the wavelength. The approach chosen by the research group at ETH Zurich, where this thesis was done, is to increase the wavelength. The currently stretched laser is emitting radiation at 3.6 μm, far above the commonly used Ti:Sapphire wavelength 800 nm, thus potentially greatly increasing the cut off energy. Before designing the recompression of the laser and before any measurements can be done, the laser needs to be fully characterized.

The aim of my project was to implement a frequency resolved gating (FROG) setup, capable of measuring a spectrally resolved autocorrelation of the pulse. The setup was used for measuring and fully characterizing the laser pulse in the mid-infrared as well as measuring on the seed laser used to generate the mid-infrared laser. After a full characterization of a pulse, the group delay dispersion (GDD) can be read out. It is desirable to create a pulse with no or close to no GDD, as those pulses will have no dispersion and will be the shortest possible with the available spectrum

The FROG setup was designed for two different wavelengths 1.07 and 3.6 μm, and therefore the beamsplitters and nonlinear crystals had to be customized for those two wavelengths. The monochromator used, as well as the stepper motor, were calibrated. A computer program was written to control the recording of the FROG traces.

When the measurements started, it was found that the laser suffered from instabilities that posed a great challenge when measuring longer traces. The monochromator used was a scanning monochromator, needing long scan times, thus further increasing the influences of the instabilities. To minimize the influence of outside noise measurements were made during the late afternoon and during the night. Furthermore, the still present noise was removed manually through manipulation of the data, giving acceptable traces.

When trying to find the optimal position (no GDD) of a prism in the seed laser, a change in lasing mode was observed. The different modes showed different temporal full width half maximum (FWHM). This is an important discovery as the shortest possible pulse (the one with shortest FWHM) is what we want to achieve. By measuring the GDD of the pulse after propagation through the prism, it could be concluded that the optimal position of the prism was outside its travel length. There exists a residual GDD of 1000 fs^2 at the optimal position of the prism.

As mentioned earlier, severe instabilities on the laser were noticed during the measurements on the mid-infrared laser. It was concluded that, before any use in experiments could be made, the laser needed to be stabilized. The measurements made were limited by the instabilities of the laser, and only estimates of the real values of the FWHM and GDD can be made. The currently stretched laser pulse in the mid-infrared was determined to have a temporal full width half maximum (FWHM) of 2.3 ps, a spectral FWHM of 200 nm and a GDD of 100000 fs^2. For recompressing the laser pulse, silicon prism compressors could be used.

Contents

1 Introduction

In today's research, high order harmonic generation(HHG)[1] is well established as a source for extreme ultraviolet laser pulses. High order harmonics are generated by atoms in a strong laser field, which respond in a highly nonlinear way, emitting high order harmonics. The emission spectra of the atoms show a long plateau, with harmonics of comparable intensities, followed by a sharp cut-off. To increase the cut off energy one can either increase the power of the laser upp to a certain point or go to longer wavelengths.

Most HHG systems are based on Ti:Sapphire based laser systems operating at 800 nm. Increasing the power for the 800 nm systems has become very expensive and as a result, new lasers with longer wavelengths are being developed. This is what is being done by the group at ETH Zurich where this thesis was done. The laser system is capable of producing laser pulses with energies of 1 μJ at 3.6 μm with a repetition rate of 100 kHz. The spectrum of the laser supports pulses down to 50 to 100 fs. Once recompressed, peak intensity sufficiently high for conducting high field physics and attosecond science will be obtained. To generate light pulses in the mid-infrared, difference-frequency generation is used from a compact fiber source[2], which is then pumped in two stages of optical parametric amplification from 1.1 mW up to 100 mW.

For optimal design of the recompression of the laser pulses, the pulse has to be fully characterized. There is also the need for later characterization of the compressed pulse before it is used in experiments. Up to date, there exist two major techniques for measuring ultra short laser pulses. Those are frequency resolved optical gating (FROG)[3], and spectral phase interferometry for direct electric-field reconstruction (SPIDER)[4]. The FROG technique is however far easier to build for different frequencies. Therefore it was chosen over SPIDER, as it was necessary to measure on the compact fiber source as well as the mid-infrared laser system.

The goal of this thesis is to build a FROG capable of measuring both the compressed fiber sources, 1.07 μm, as well as the mid-infrared radiation, 3.6 μm, fully characterizing the mid-infrared pulse.

2 Theory

The simplest and most conventional way to describe the electromagnetic field in a laser pulse is by omitting the magnetic part and only presenting the electric part of the field without z dependence as following:

$$E(t) = A(t)\exp(i\omega_0 t)\exp(i\varphi(t)), \tag{2.1}$$

where A(t) is the absolute value of the electric field, |E(t)|, also called the envelope of the pulse. The square of the amplitude of the electric field is proportional to the intensity, $A^2(t) \propto I(t)$, which is the most easily measured property of an electric field. The angular frequency, ω_0, can be chosen arbitrarily, but it is mostly chosen at the center of the pulse spectrum. The time dependent phase $\varphi(t)$ on the other hand is far more difficult to measure, and contains information on the frequencies dispersion in time. The derivative of the phase, $d\varphi(t)/dt$, gives information about how the frequencies of the pulse change as a function of time.

It is desirable, when trying to create as short pulses as possible, to obtain a pulse with zero chirp, whereas a pulse with positive or negative chirp will have its pulse shape distorted and broadened. Adding a chirp to a pulse should be avoided unless one needs to add the chirp to compensate for an already present chirp with the opposite sign.

The electric field can, just as in the time domain, be defined in the frequency domain as

$$\tilde{E}(\omega) = \tilde{A}(\omega)\exp(i\varphi(\omega)), \tag{2.2}$$

where $\tilde{A}(\omega)$ denotes the spectral amplitude and $\varphi(\omega)$ the spectral phase. The square of the spectral amplitude is proportional to $S(\omega)$, the spectral density, or simply, the spectrum of the electric field, with $\tilde{A}^2(\omega) \propto S(\omega)$.

The frequency domain representation of the electric field can be obtained through the Fourier transform:

$$\tilde{E}(\omega) = \frac{1}{\sqrt{2\pi}} \int_{-\infty}^{\infty} E(t)\exp(i\omega t)dt \tag{2.3}$$

The inverse Fourier transform transforms the electric field from the frequency domain back to the time domain.

$$E(t) = \frac{1}{\sqrt{2\pi}} \int_{-\infty}^{\infty} \tilde{E}(\omega)\exp(-i\omega t)d\omega \tag{2.4}$$

When passing through a dispersive media, such as glass where the refractive index n depends on the frequency, the electric field in a laser pulse acquires a spectral phase:

$$\varphi(\omega)=\frac{\omega}{c}n(\omega)L\,, \tag{2.5}$$

with L, the length of the medium, and c, the speed of light. The phase gained through propagation in a dispersive media is added to the already present phase. The first and second derivative of the spectral phase give two important quantities: The group delay, $\tau_g(\omega)$, and the group delay dispersion, GDD(ω). The group delay gives the difference in time delay aquired by the different frequencies when passing through a dispersive medium. The group delay dispersion describes how the group delay varies with frequency, broadening the pulse and giving it a chirp. There exist a strong relationship between chirp and GDD. If a pulse shows any GDD it will also have a chirp.

One way of easily controlling whether a pulse has a chirp(and GDD) or not is by measuring its temporal duration and spectral width in the frequency domain and multiply it with one another. For a true Gaussian-shaped pulse, without any chirp, the time-bandwidth product (TBP) is approximately 0.44 and for a sech^2-shaped pulse the TBP should be 0.315. A pulse without a chirp is referred to as bandwidth limited.

The Wigner distribution is the representation of an ultra short laser pulse by a function in time-frequency space, W(t,ω). The Wigner function in the time domain is defined as follows:

$$W(t,\omega)=\frac{1}{\sqrt{2\pi}}\int_{-\infty}^{\infty}E\left(t+\frac{t'}{2}\right)E^*\left(t-\frac{t'}{2}\right)\exp(i\omega t')dt' \tag{2.6}$$

It allows for a better representation of the laser pulse than normally obtained by using the description of the electric field in time or frequency. It also gives an easier understanding of what the addition of GDD means for a laser pulse. Another characteristic of the Wigner distribution is that integrating over time or frequency will give the spectrum respectively the pulse intensity of the electric field.

$$I(t)=|E(t)|^2=\int_{-\infty}^{\infty}W(t,\omega)d\omega \tag{2.7}$$

$$I(\omega)=|E(\omega)|^2=\int_{-\infty}^{\infty}W(t,\omega)dt \tag{2.8}$$

What is measured by a FROG setup, a spectrally resolved autocorrelation, is also time-frequency dependent.

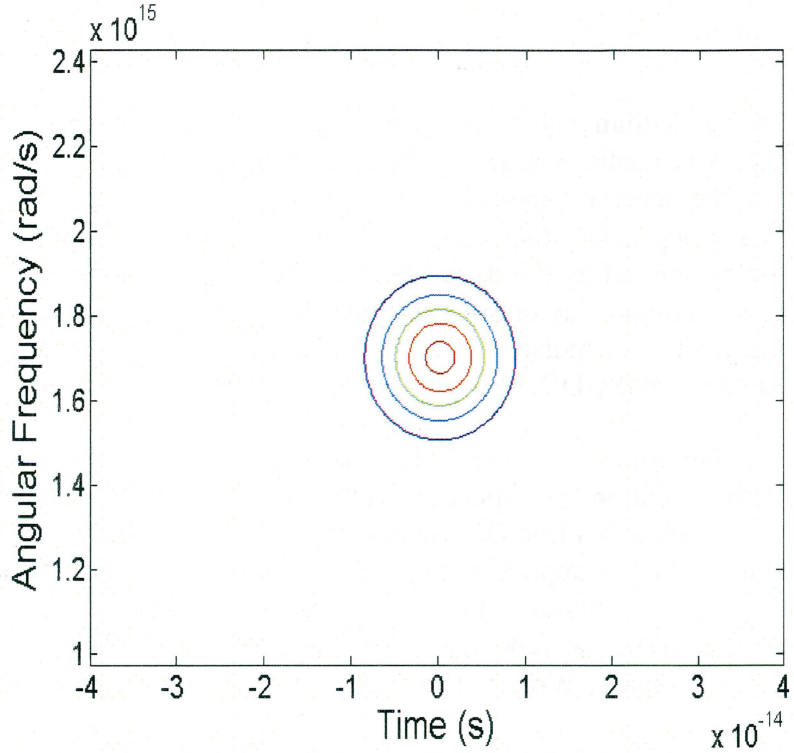

Figure 1. Wigner distribution of a bandwidth limited Gaussian pulse, centered at around 1100nm.

The Wigner distribution of a bandwidth limited pulse is perfectly symmetrical, but as one lets it propagate through a material, the effects of group delay, $\tau_g(\omega)$, and group delay dispersion, GDD(ω), become visible.

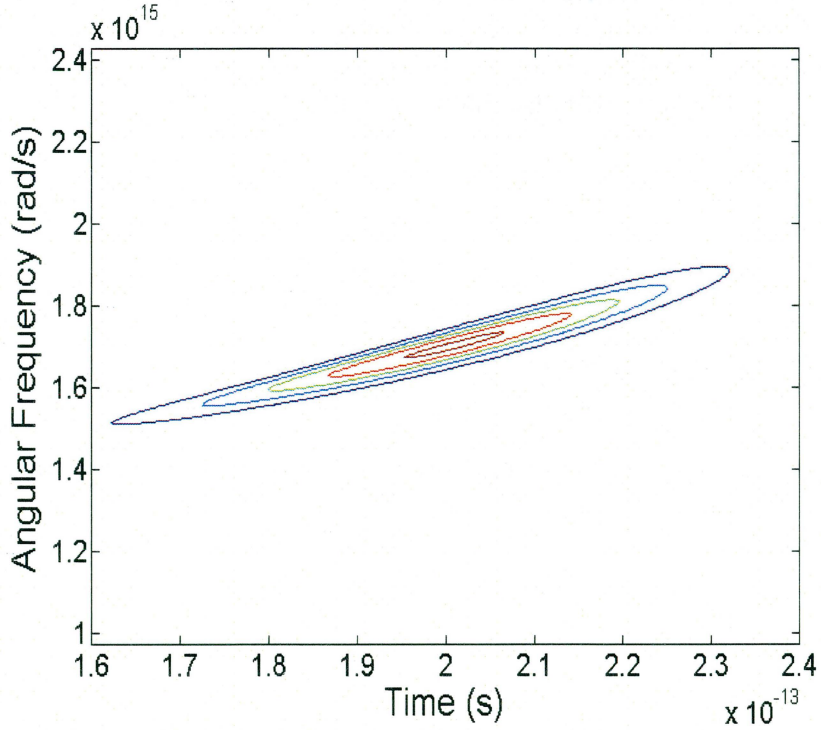

Figure 2. The Wigner distribution of a Gaussian-shaped pulse, centered around 1100 nm, after propagation trough 3 mm of borosilicate Schott glass, BK7, clearly showing the GDD added to the pulse by the material as well as the group delay obtained.

The effect of propagation through the material is clearly visible in the Wigner plot above. A group delay of around 0.2 ps and a strong GDD have been added and can be seen in the plot. The red part of the spectrum exits the dispersive medium first, with a delay of 0.16 ps, and the blue part of the spectrum last, with a delay of 0.23 ps.

2.1 Harmonic Generation

The susceptibility of a media, χ, describes how strongly it gets polarized when exposed to an electric field. In vector form the equation can be written as following:

$$\vec{P}(t) = \varepsilon_0 \chi \vec{E}(t), \tag{2.9}$$

with ε_0 the electric permittivity of free space, **P**(t) the polarization and **E**(t) the electric field. The induced polarization in the material acts as a driving polarization that itself induces an electric field with linear and nonlinear components. The equation (2.9) is normally generalized into a power series of **P**(t) in the field strength **E**(t) as

$$\vec{P}(t) = \varepsilon_0 \left(\chi^{(1)} E(t) + \chi^{(2)} E^2(t) + \chi^{(3)} E^3(t) + \chi^{(4)} E^4(t) + \ldots \right). \tag{2.10}$$

The real part of the linear susceptibility $\chi^{(1)}$ gives the speed in the optical media, whereas the imaginary part gives the absorption in the medium. The terms $\chi^{(2)}$ and $\chi^{(3)}$ are the second- and third-order nonlinear optical susceptibilities. The second order nonlinear polarization

$$\vec{P}^{(2)}(t) = \varepsilon_0 \chi^{(2)} \vec{E}^2(t) \tag{2.11}$$

gives rise to nonlinear effects such as sum frequency generation (SFG) and second harmonic generation (SHG). In this thesis, the dominant and most important nonlinear effect is the second harmonic generation.

2.1.1 Second Harmonic Generation

The polarization of a second order nonlinear process is given by

$$\vec{P}^{\omega_3}(t) = \varepsilon_0 \chi^{(2)}(-\omega_3, \omega_2, \omega_1) \vec{E}^{\omega_2}(t) \vec{E}^{\omega_1}(t) \tag{2.12}$$

where

$$\omega_1 + \omega_2 = \omega_3 . \tag{2.13}$$

Equation (2.13) is valid for both SFG and SHG. For second harmonic generation ω_1 is equal to ω_2 and $\omega_3 = 2\omega_1$.

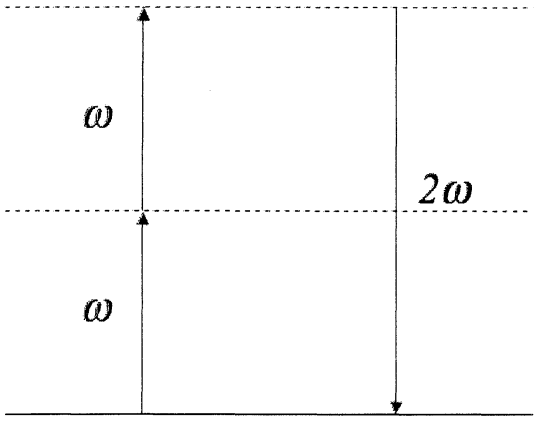

Figure 3. An energy level diagram describing second harmonic generation. The atom absorbs two photons with angular frequency ω in a short time interval and sends out a photon with angular frequency 2ω. The solid line represents the ground state and the dashed lines virtual states.

A common convention within nonlinear optics is to write the second order susceptibility, χ, see equation (2.11), as a first order tensor written as 2d, see equation (2.14). The second order susceptibility is thus a third order tensor. Due to symmetrical reasons the nonlinear susceptibility tensor can be represented by a 3x6 matrix with the value of the components being material dependent.

For a fixed geometry, fixed propagation and polarization direction, the expression for the second harmonic generation (2.12) can be replaced by a scalar relation:

$$P(2\omega) = \varepsilon_0 2 d_{eff} E^2(\omega) \tag{2.14}$$

The value of d_{eff} depends on the alignment of the crystal and is thus dependent on the two spherical angles θ and ϕ. The exact expression of d_{eff} for different nonlinear crystals can be found in the literature.

With the z dependence not omitted from equation (2.1) and the nonlinear polarization used as a source term in Maxwell's equations one can obtain the following expression for the intensity of the generated second harmonic:

$$I(2\omega) = \frac{2\omega^2 d_{eff}^2 L^2}{\varepsilon_0 c^3 n_3 n_1^2} I^2(\omega) \sin c^2\left(\frac{\Delta k L}{2}\right) \text{[5]}, \tag{2.15}$$

with the wavevector mismatch

$$\Delta k = 2k_1 - k_3 . \tag{2.16}$$

Here n_3 and n_1 are the different refractive indexes seen by the generated second harmonic, ω_3, and the original frequency, ω_1. From equation (2.15) one can conclude that the intensity of the generated second harmonic will be greatest when the wavevector mismatch is equal to zero, $\Delta k=0$, as seen in figure 4.

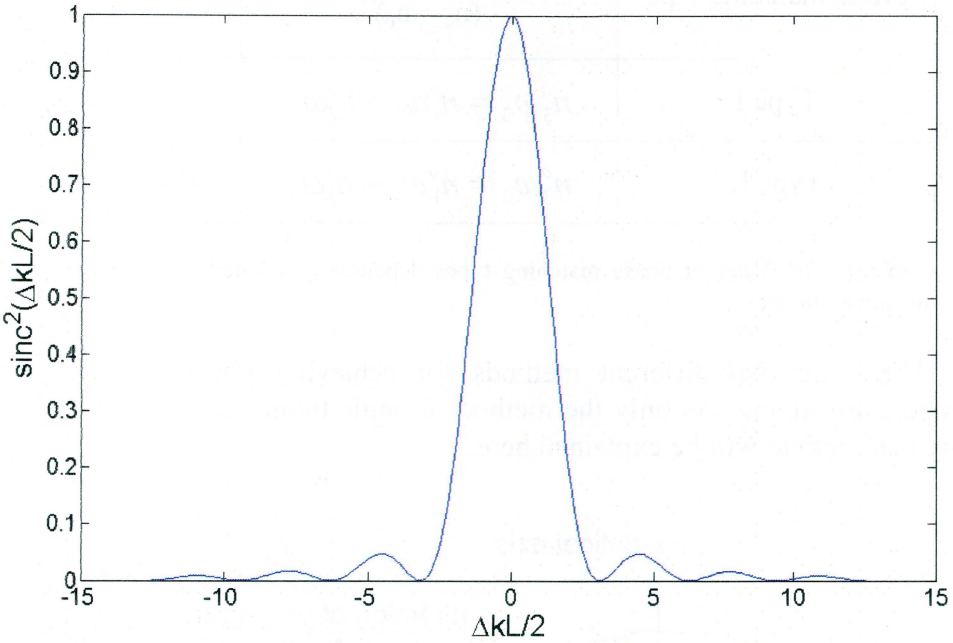

Figure 4. The effects of a too large wavevector mismatch will lead to a very low power of the generated second harmonic signal.

For Δk to be zero, the condition for optimal SHG, the relation between the different refractive indexes can be derived as follows:

$$\Delta k = 2k_{\omega} - k_{2\omega} = 2\left(2\pi n_{\omega}/\lambda\right) - 2\pi n_{2\omega}/\left(\lambda/2\right) = 0 \Rightarrow$$

$$n_{\omega} = n_{2\omega} \tag{2.17}$$

To maximize the SHG, one has to match the refractive of the fundamental with the generated second harmonic, called phase matching. The condition for phase matching, $\Delta k=0$, can be difficult if not impossible to achieve. This can be worked around by using the birefringence of certain crystals. Birefringence means that the refractive index of a material is dependent on the polarization of the optical radiation. Crystals with one optical axis, uniaxial crystals, have this characteristic. Depending on the polarization the beam can either see a constant refractive index, independent of the angle to the optical axis, referred to as ordinary refractive index, n_o, or a refractive index dependent on the angle, referred to as extraordinary refractive index, n_e, or a combination of both. The sign of the birefringence (n_e - n_o) determines whether the material is called negative uniaxial ($n_e < n_o$) or positive uniaxial ($n_e > n_o$). There exist two different types of phase matching, type I where the two lower frequency waves have the same polarization and type II where they have orthogonal polarizations.

Phase matching type	Positive uniaxial ($n_e > n_o$)	Negative uniaxial ($n_e < n_o$)
Type I	$n_3^o\omega_3 = n_1^e\omega_1 + n_2^e\omega_2$	$n_3^e\omega_3 = n_1^o\omega_1 + n_2^o\omega_2$
Type II	$n_3^o\omega_3 = n_1^o\omega_1 + n_2^e\omega_2$	$n_3^e\omega_3 = n_1^e\omega_1 + n_2^o\omega_2$

Table 1. The different phase matching types depending on whether the material is positive or negative uniaxial.

There are two different methods for achieving phase matching, angle and temperature tuning. As only the method of angle tuning was used within the thesis, only that method will be explained here.

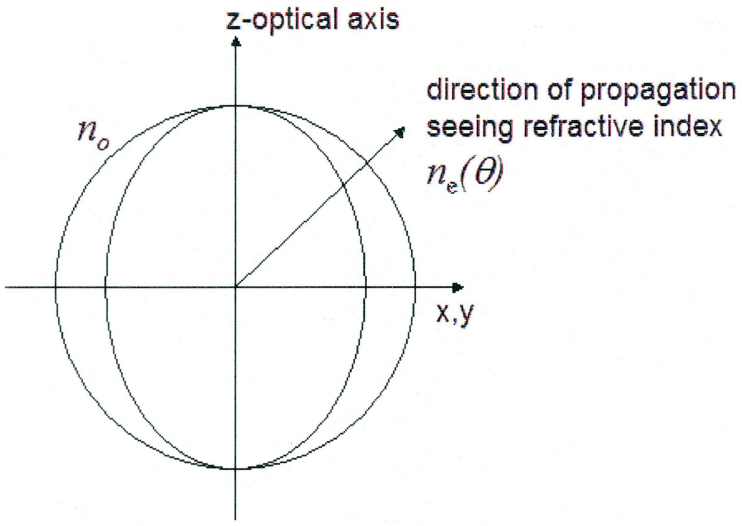

Figure 5. The refractive index ellipsoid. Depending on the polarization and propagation direction, the laser pulse sees a different refractive index depending on both n_o and $n_e(\theta)$. By tuning the angle, one can satisfy the condition for phase matching $\Delta k=0$.

To calculate the angle needed for type I phase matching one starts with the equation of an ellipse:

$$\frac{1}{n_e^2(2\omega,\theta)} = \frac{\sin^2(\theta)}{n_e^2(2\omega)} + \frac{\cos^2(\theta)}{n_0^2(2\omega)} \tag{2.18}$$

by choosing the angle θ to satisfy equation (2.17) we have:

$$n_e(\theta,2\omega) = n_0(\omega) \tag{2.19}$$

and we arrive at:

$$\frac{1}{n_0^2(\omega)} = \frac{\sin^2(\theta)}{n_e^2(2\omega)} + \frac{\cos^2(\theta)}{n_0^2(2\omega)} \tag{2.20}$$

by solving for $\sin^2\theta$ we finally arrive at:

$$\sin^2(\theta) = \frac{\frac{1}{n_0^2(\omega)} - \frac{1}{n_0^2(2\omega)}}{\frac{1}{n_e^2(2\omega)} - \frac{1}{n_0^2(2\omega)}} \tag{2.21}$$

When the angle θ has been found for optimization of the SHG, the refractive index of the generated second harmonic, n"(2ω), can be derived from equation (2.18) to be:

$$n_e(\theta,2\omega) = \left(\frac{\sin^2(\theta)}{n_e^2(2\omega)} + \frac{\cos^2(\theta)}{n_0^2(2\omega)}\right)^{-\frac{1}{2}} \tag{2.22}$$

2.1.2 High order Harmonic Generation

While generating second- and third-order harmonics uses nonlinear crystals, the generation of far higher harmonics, so called high order harmonics (HHG)[1], requires a different approach. When focusing an intense and extremely short laser pulse onto an atomic gas, one gets a nonlinear response from the atoms; coherent light being emitted from the atoms in multiples of the original frequency is generated.

The multiple frequencies generated shows constant power over a certain spectral range, the plateau, up to a cutoff frequency where the power of the generated HHG suddenly drops.

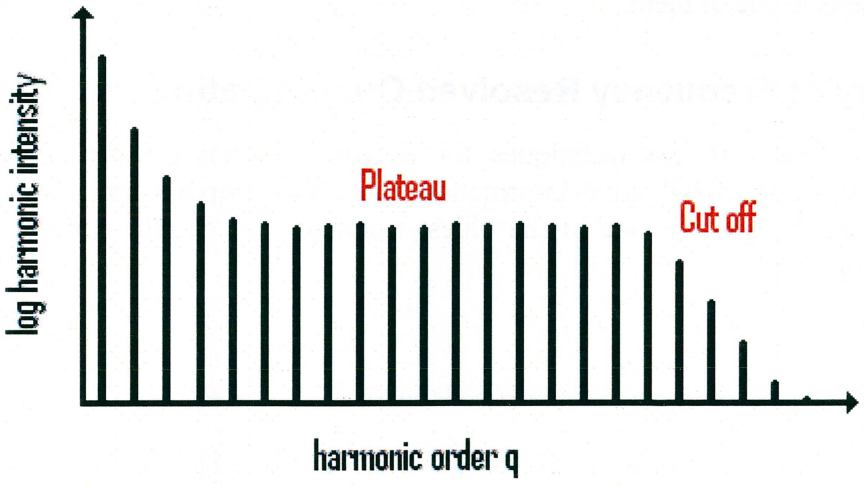

Figure 6. The power of the generated high order harmonics is stable over a large region, called the plateau, up to a point where the power suddenly drops, the cut off.

By combining the different generated high order harmonics and letting them interfere with one another, extremely short pulses, shorter than two hundred attoseconds[6], can be generated. The shorter the pulse, the shorter time resolution

can be achieved when using the pulse for measuring on different physical systems. To be able to, for example, take a 'picture' of an electron circulating around its atom in Bohr's atom model, one would need a time resolution of a few tenths of attoseconds. This number can be derived from assuming the electron is circulating the atom at a distance equal to the Bohr radius, the so called Bohr-Model, with a velocity and time of flight for one circulation of the nucleus as calculated below by dividing the Bohr radius by the velocity the electron has in the classical model[1].

$$\frac{2\pi r}{v} = \frac{2\pi * 0.53\mathring{A}}{v}, \quad with \ v = \sqrt{\frac{e^2}{4\pi\varepsilon_0 mr}} \Rightarrow \frac{2\omega r}{v} \approx 150as \tag{2.23}$$

To be able to get a high enough resolution for an event that takes around 150 as one needs a pulse of around 10 as. To generate that short pulses with HHG, the cutoff energy needs to be pushed up to over 1 keV[7]. To reach a higher and higher cutoff energy in the harmonic spectra, one can either increase the amplitude of the laser, or one can increase the wavelength. This can be seen in the following two equations:

$$E_{cutoff} = I_P + 3.17U_P \tag{2.24}$$

The atomic ionization potential, I_P, is material dependent and cannot be influenced, but the ponderomotive energy, U_P, can. The ponderomotive energy depends on the energy of the laser pulse and the wavelength:

$$U_P = \frac{e^2 E_0^2}{4 m_e \omega^2} \propto I * \lambda^2 \tag{2.25}$$

As the increase in the cutoff energy scales to the power of two with the wavelength, and the laser at around 800 nm normally used for HHG is becoming harder to push to higher powers, new lasers with high powers in the mid-infrared regime, increasing the wavelength increases the ponderomotive energy, are being developed. The laser used within this thesis is one of them.

2.2 Theory of Frequency Resolved Optical Gating

There exist several different techniques for measuring ultrashort optical pulses. Intensity autocorrelation will give information about the temporal structure of the pulse and, even though it is one of the oldest techniques, it is still used for pulse characterization today.

[1] The electron is held in place at an orbit around the nucleus where the centripetal force is given by the Coulomb force.

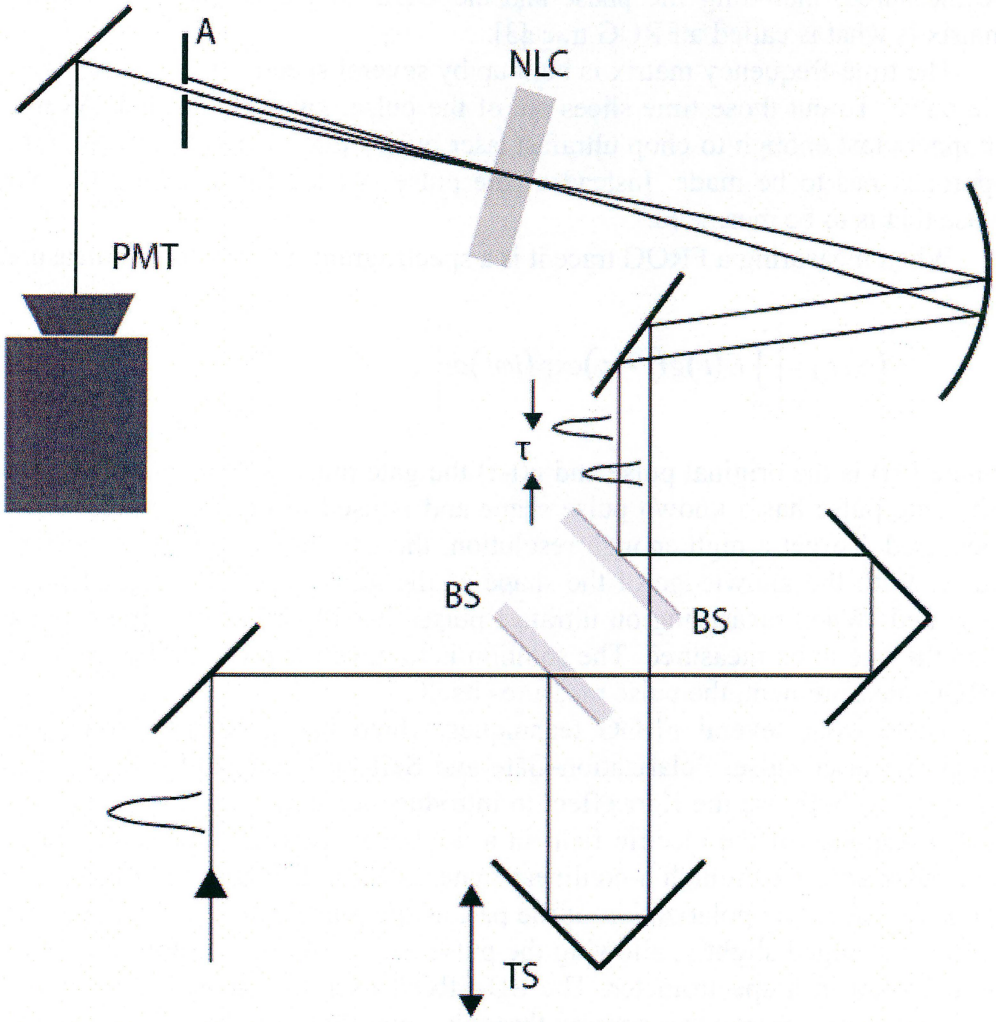

Figure 7. Figure showing the setup of a background free intensity autocorrelation. The laser pulse is split into two parts by the beamsplitters, BS. The motorized translation stage, TS, changes the delay, τ, between the two parts of the laser pulse coming from the beamsplitters. The two laser pulses are focused together by a curved mirror onto the nonlinear crystal, denoted NLC. There, the generated direct SH, that is later blocked by an aperture, A, is created along with a SHG from the interaction of the two beams. The SHG from the interference of the beams pass through the aperture into the photomultiplier, PMT, where it is measured.

The limitation of the intensity autocorrelation is that to recreate the original pulse shape from the measured intensity autocorrelation, I_{ac};

$$I_{ac} \propto \int_{-\infty}^{\infty} |E(t)E(t-\tau)|^2 \, dt = \int_{-\infty}^{\infty} I(t)I(t-\tau)dt \,, \tag{2.26}$$

one has to assume a pulse without chirp or only a linear chirp with unknown sign of the chirp. Furthermore, the intensity autocorrelation is somewhat insensitive to the shape of the pulse. Several slightly different pulse shapes will give the same intensity autocorrelation. Only if the real pulse shape is known can the autocorrelation be used to measure the pulse duration. However, this is normally not the case. To gain more information a spectrum can be recorded at every time delay. The time-frequency matrix measured can be used to recreate the original pulse and the pulse duration can

be measured, including the phase and the GDD of the pulse. This time-frequency matrix is what is called a FROG trace[3].

The time-frequency matrix is built up by several spectrally resolved time slices of the pulse. To cut those time slices out of the pulse, gating is needed. As mechanical choppers fast enough to chop ultrafast laser pulses into pieces do not exist a different approach has to be made. Instead a gate pulse is used for selecting the part of the pulse that is to be measured.

When measuring a FROG trace it is a spectrogram, $S(\omega,\tau)$, that is measured.

$$S(\omega,\tau)=\left|\int_{-\infty}^{\infty}E(t)g(t-\tau)\exp(i\omega t)dt\right|^2, \tag{2.27}$$

where E(t) is the original pulse and $g(t-\tau)$ the gate pulse with a variable time delay, τ. The gate pulse has a known pulse shape and is used to probe the pulse that is to be measured. To get a high enough resolution, the gate pulse has to be shorter than the pulse. With the knowledge of the shape of the gate pulse, the original pulse can be recreated. When measuring on ultrafast pulses it will be hard to find a pulse shorter than the one to be measured. The solution is to have the pulse probe itself. Thus, in a FROG measurement, the pulse measures itself.

There exist several FROG techniques which use different physical effects to probe the laser pulse. Polarization-Gate and Self-Diffraction FROG (PG-FROG and SD-FROG) both use the Kerr effect to introduce a change in the refractive index due to the response of the electric field in a nonlinear material. In PG-FROG the probe and pulse are sent through a nonlinear material with different polarizations. Through the Kerr effect, the polarization of the part of the pulse which is overlapping with the probe is changed slightly, allowing the pulse to pass through a polarizer where it can be recorded in a spectrometer. The SD-FROG uses the sinusoidal intensity pattern created by two laser pulses passing through a material to induce a sinusoidal index of refractive grating in the material. The grating diffracts parts of each beam, and the part of the pulse that is diffracted can be measured. For second-harmonic generation FROG (SHG-FROG) the probe and laser beams are made to overlap in a nonlinear material and the second harmonic generated from the overlap between the pulse and probe is measured.

For SHG-FROG the gate pulse can be rewritten as $E(t-\tau)$.

$$S(\omega,\tau)=\left|\int_{-\infty}^{\infty}E(t)E(t-\tau)\exp(i\omega t)dt\right|^2 \tag{2.28}$$

3 Generation of Mid-Infrared Laser Pulses

The laser system used for generating laser pulses at a frequency in the infrared uses a chirped pulse optical parametric amplifier (CPOPA)[8] to generate few-cycle pulses in the mid-infrared. An erbium doped fiber laser amplifier is used to generate 2 laser beams at 1585 nm, pulse durations of 65 fs at a repetition rate of 82 MHz. One of the beams is passed through a highly nonlinear fiber (HNLF)[9] where a white light continuum is generated. The short wavelength part is tunable between 1.05 and 1.4 μm. In our experiment only the wavelength range between 1.05 and 1.18 μm is used. By first spatially separating the frequency components from the HNLF with two prisms, one can cut away part of the spectrum by inserting a knife blade into the beam. The two laser beams are recombined through a beamcombiner, and through difference frequency generation (DFG) mid-infrared radiation is generated.

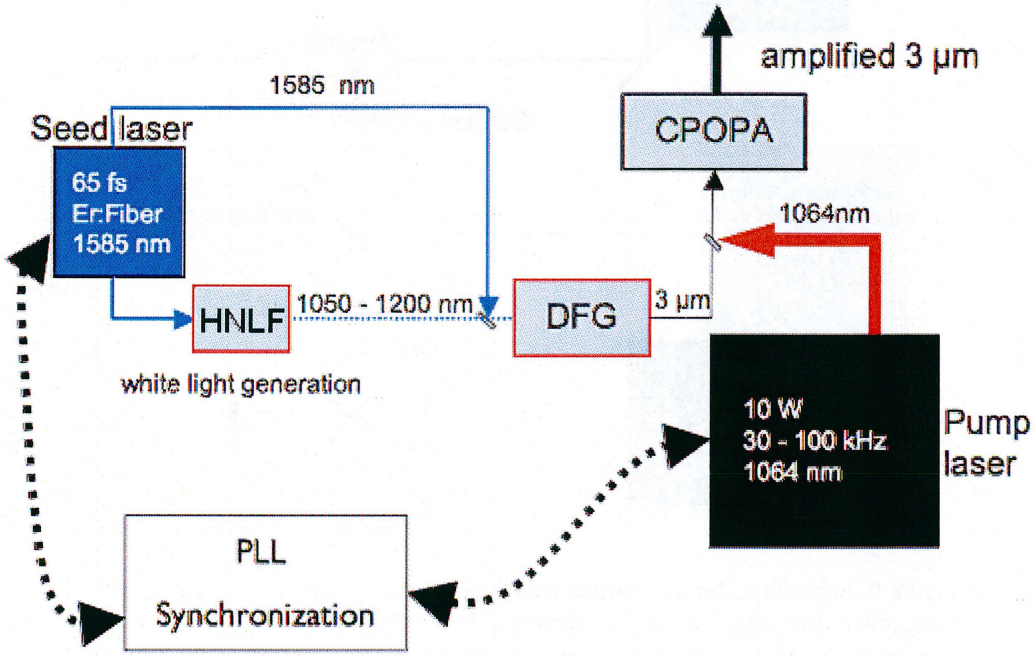

Figure 8. Schematic picture of the setup of the difference frequency generation to obtain Mid-IR radiation. The erbium doped fiber laser generates radiation at 1585 nm with one beam passing through a highly nonlinear fiber (HNLF), generating white light. Through difference frequency generation (DFG), a laser beam at 3 μm, which is later amplified by a CPOPA is generated. The fiber laser and the pump laser are synchronized through a Phase locked loop (PLL)[10].

The laser pulse propagating through the HNLF will acquire some GDD. To counter the added GDD, material is introduced into the beam giving the opposite sign of the GDD, compared to the HNLF. This can be done by moving more or less of the prisms positioned after the HNLF into the beam.

The laser pulse going through the HNLF and the prisms was sent into the FROG setup to characterize it, measuring the FWHM and GDD of the pulse. This was done while changing the position of the prism in the beam to find the optimal position, i.e. to find the pulse with the smallest FWHM, or the pulse with no GDD.

After the mid-infrared radiation has been generated through DFG, the laser pulse gets amplified in two stages through chirped pulse optical parametric amplification, CPOPA.

The pump laser has an output power at 1 W with a repetition rate of 82 MHz at a wavelength of 1064 nm. A pockels cell is placed in the beam path and blocks the beam, only letting through every 800th pulse from the seed laser, which is then subsequently amplified. The amplified laser beam ends up with a repetition rate at around 100 kHz and 10 W of output power. When combining the generated mid-infrared radiation with the pump laser, a third wavelength is generated. For 3.6 μm the generated third wavelength is 1.6 μm. The two wavelengths, 3.6 and 1.6 μm, are both amplified by the pump laser. All frequencies, but the mid-infrared, are blocked before any measurements are done.

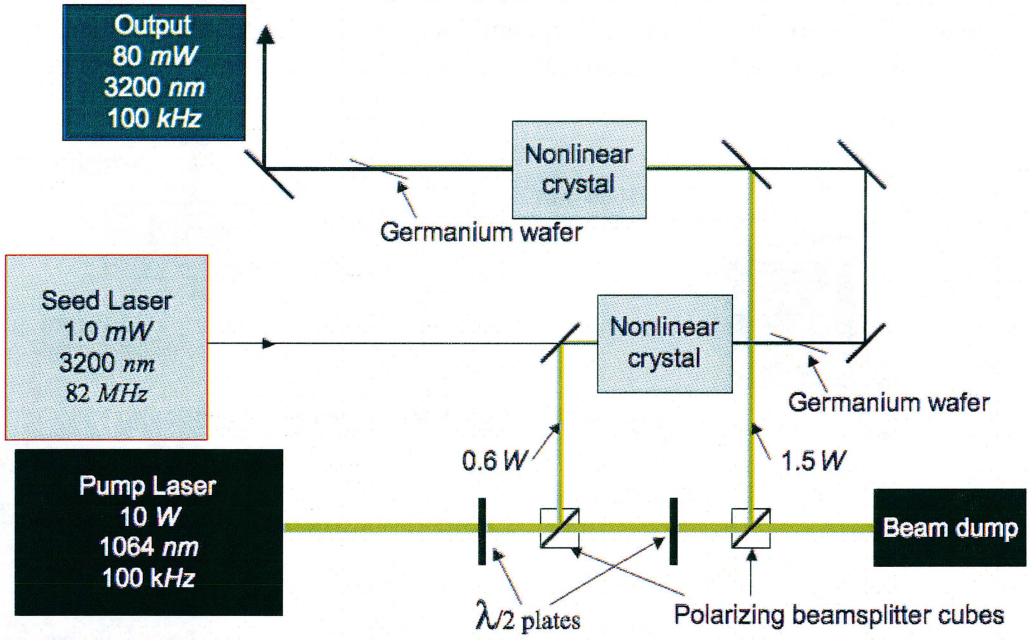

Figure 9. Schematics for the chirped pulse optical parametric amplification, CPOPA. The 3.6 μm laser pulse gets amplified in two steps by the pump laser. The amount of power sent into the nonlinear crystals by the pump laser is controlled by two λ/2 plates and the following polarizing beamsplitter cubes. Germanium wafers are used to block off all radiation except the generated 3.6 μm giving a final output of the laser of 100 mW pulses at 100 kHz.

4 Setup for Frequency Resolved Optical Gating

In this thesis a FROG setup was designed and created for two purposes, to characterize parts of the seed laser and to characterize the mid-infrared laser. To The setup for second-harmonic generation FROG (SHG FROG) is a background free intensity autocorrelation combined with a spectrometer at its output. It is capable of recording the temporal and spectra profile of the nonlinear signal (Fig. 10).

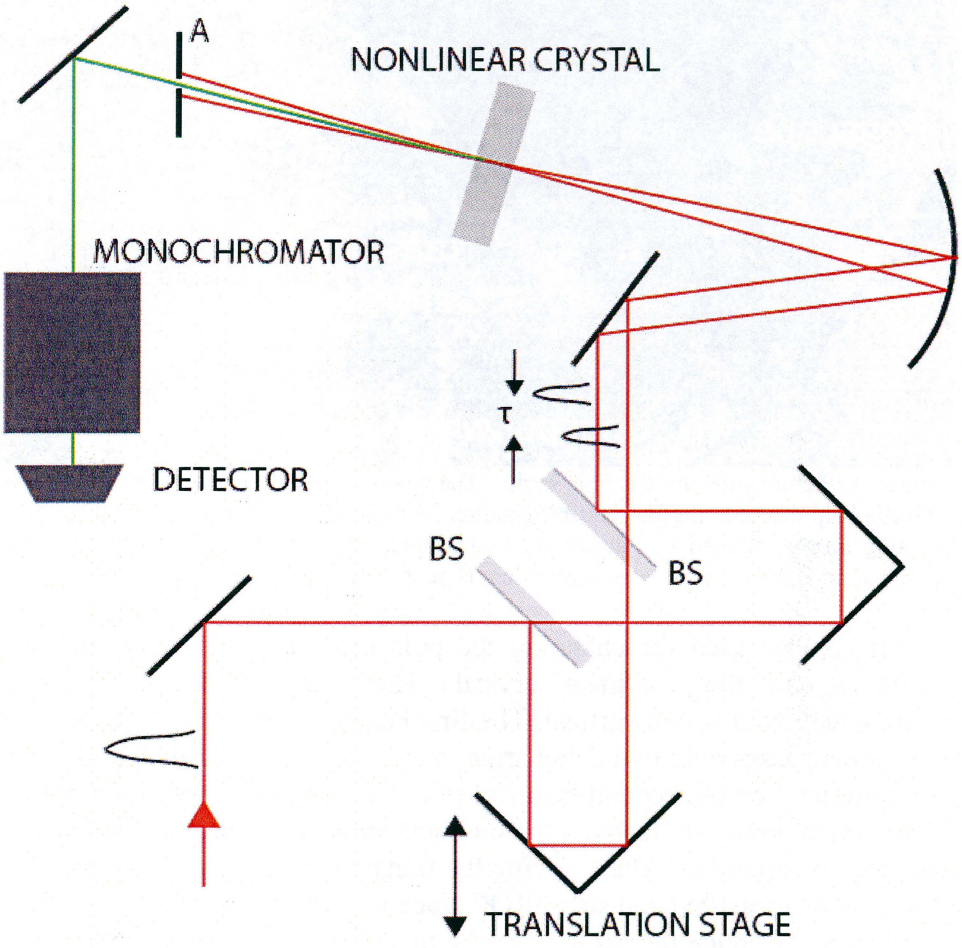

Figure 10. Setup of SHG FROG. The beamsplitters, BS, one mounted on a translation stage, TS, splits the beam in two and recombines them again before a curved mirror focuses the beams into the nonlinear crystal, NLC. An aperture, A, blocks off the unwanted parts of the beam.

The laser pulse is split into two parts by the beamsplitters. The motorized translation stage changes the delay, τ, between the two parts of the laser pulse coming from the beamsplitters. The two laser pulses are focused together by a curved mirror onto the nonlinear crystal. In the crystal SHG happen either directly by each laser pulse or through the interaction between the two laser pulses. The direct SHG is eliminated by an aperture. The SHG from the interaction of the two beams passes through the aperture into the monochromator, where the beam is split up into its frequency components before being detected.

What the real setup looks like can be seen in the following picture.

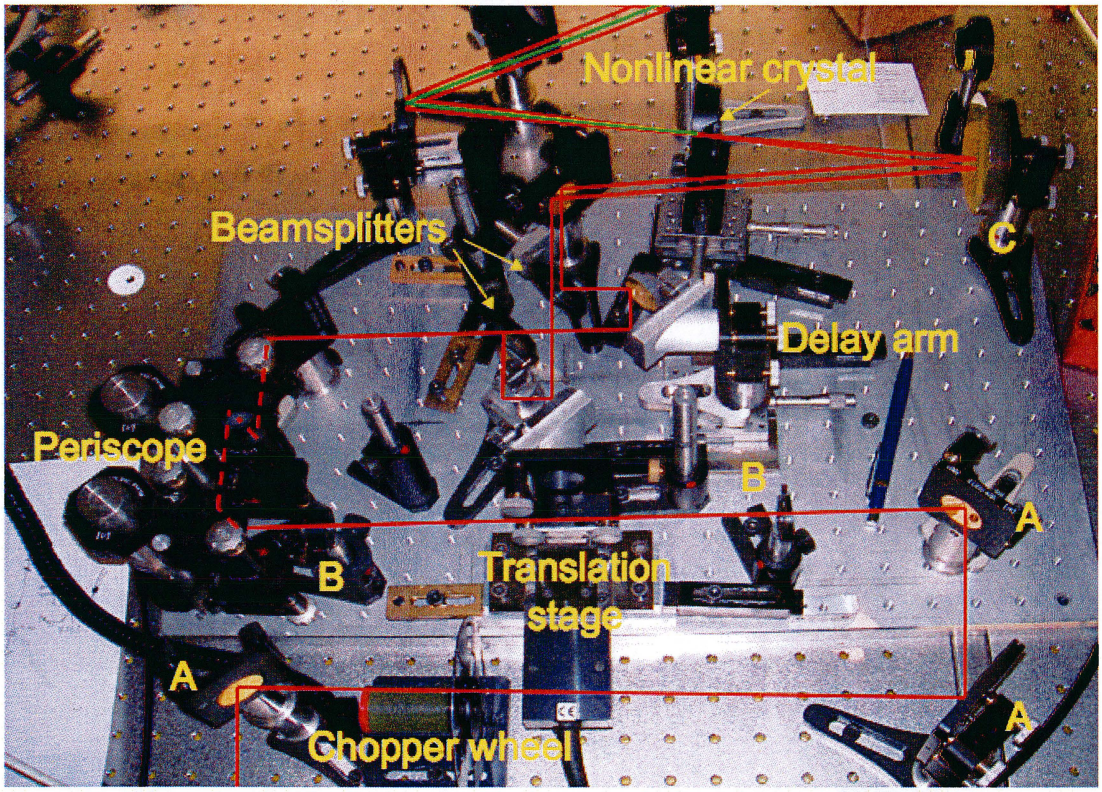

Figure 11. Picture showing the final setup. The beam, marked red, is sent in to the FROG setup with the help of three aligning mirrors, marked with an A, and with two pinholes, marked B. A focusing mirror, marked C, focuses the two beams, after passing over the delay arms into the nonlinear crystal where the second harmonic is generated, marked green.

A periscope is used for changing the polarization of the laser beam to fit the beamsplitters and the nonlinear crystal. The beam enters with a horizontal polarization and exits with a vertical. The first beamsplitter splits the beam in half and the two beams passes over two delay arms, one mounted on a translation stage, before being recombined on the second beamsplitter. The second harmonic generated in the nonlinear crystal is sent in through the monochromator, not seen on the picture, and a spectrum can be recorded. After moving the translations stage one step forward a new spectrum can be measured and so a FROG trace is slowly recorded

I will now introduce the setup with the theoretical simulations that were done to account for each element. As the FROG setup was designed for two different frequencies, 1.07 and 3.6 μm, a few of the components had to be changed in the setup when changing from measuring on one of the lasers to the other one.

4.1 Beamsplitters

The beamsplitters are used to split the beam in two equal parts. There are, unfortunately, no beamsplitters that will work in a frequency range broad enough for both lasers that were measured with in this work, so the beamsplitters had to be changed when changing between the two frequencies.

4.1.1 Beamsplitters for the Laser at 1.07 μm

For the laser at around 1.07 μm a beamsplitter made out of borosilicate Schott glass, or BK7, was chosen. To investigate the amount of dispersion that the beamsplitters add and the resulting pulse broadening a simulation was performed. A bandwidth limited Gaussian pulse centered around 1.07 μm with a temporal full width half maximum (FWHM) of around 20 fs was propagated through two beamsplitters at an angle of 45 degrees. At a thickness of approximately 14 mm BK7 glass the dispersion added to the pulse broadened the pulse with no more than 6%. As the pulse measured turned out to be far larger than 20 fs and because other larger error sources, see chapter 5, the dispersion could be ignored.

4.1.2 Beamsplitters for the Laser at 3.6 μm

For the laser at 3.6 μm beamsplitters of the material Calcium Fluoride, CaF_2, were used. The thickness of the beamsplitters were 1 mm and the width of the pulses at 3.6 μm was almost 1000 times broader than the pulses at 1.07 μm, with a FWHM of around 20 ps. There should therefore be no visible dispersion whatsoever of the pulse, as also shown by the simulations, with such a broad pulse.

The dispersion of the wavelength at 3.6 μm can be ignored as it will not increase the error of the measurements.

4.2 Nonlinear Crystals

The nonlinear crystal plays an important role inside the FROG setup and has therefore to be designed properly. If designed with a too small thickness the nonlinear efficiency will become too low, as can be seen in equation (2.15). Dividing the thickness by two will divide the efficiency by four. Equation (2.15) also shows that increasing the thickness will create a smaller bandwidth of the area where effective SHG can occur. Increasing the thickness will narrow the sinc-function seen in figure 4. One needs to find a balance between high efficiency and a large bandwidth.

For deciding what crystals to use for SHG at the two wavelengths 1.07 and 3.6 μm a freeware computer program, called SNLO, was used. Depending on the orientation of the crystal the laser beams will pass through the crystal seeing an effective nonlinear susceptibility tensor, d_{eff}, as described in equation (2.14), depending on the spherical angles θ and φ. The angle φ is chosen to optimize the d_{eff} and is easily calculated from the tabulated values of d_{eff} found in the literature, see table 2. From evaluating the different crystals with the SNLO program it was found that the crystal BBO was most suitable for SHG at 1.07 μm and that $AgGaS_2$ was most suitable for SHG at 3.6 μm. Both crystals show a large and broadband nonlinear efficiency at 1.07 and 3.6 μm respectively.

Crystal	d_{eff}	Optimal angle φ
BBO	$d_{eff} = d_{31}\sin(\theta+\rho) - d_{22}\cos(\theta+\rho)\sin 3\varphi$ [11]	φ = 90°
$AgGaS_2$	$d_{eff} = d_{36}\sin 2\varphi \sin\theta$ [12]	φ = 45°

Table 2. The equations for d_{eff} for the two crystals BBO and $AgGAS_2$. The optimal value of φ for maximum value on d_{eff} and therefore maximum SHG can be seen in the right column. The constants d_{31}, d_{22}, d_{36} and ρ are material dependent and can be found in the literature.

From the equations for d_{eff} in table 2 it is easy to calculate what value of the angle φ that will lead to maximum SHG. This value can also be seen in the rightmost

column of table 2. What value of θ to pick to maximize the SHG depends on the refractive index of the material at the wavelength that is to be frequency doubled. The exact formula for calculating the angle has been presented in the theory section, see equation (2.21). For calculating the angle, one needs the value of the refractive index depending on the frequency of the light passing through the crystal. This can be obtained from the Sellmeier equation. The Sellmeier equation is normally presented in one of the two following forms:

$$n^2(\lambda) = 1 + \frac{B_1\lambda^2}{\lambda^2 - C_1} + \frac{B_2\lambda^2}{\lambda^2 - C_2} + \frac{B_3\lambda^2}{\lambda^2 - C_3}, \tag{4.1}$$

or

$$n^2(\lambda) = A + \frac{B}{\lambda^2 - C} - D\lambda^2 \tag{4.2}$$

The constants belonging to the Sellmeier equation vary between the different materials and the constants for BBO[13] and $AgGaS_2$[14] can be found in the literature.

An $AgGaS_2$ crystal was used for SHG in the mid-infrared. It was ordered with a thickness of 250 μm, the angle φ was 45° and the angle θ was 90°. The dimensions of the BBO crystal were decided through simulations of the nonlinear efficiency at different wavelengths. First the angle φ was decided from the d_{eff}, as seen in table 2, to be 90°. The angle θ was calculated to be around 22.8°. The exact angle needed was also confirmed in the simulation that was run to determine the thickness of the crystal. The thickness had to be a compromise between good efficiency and large bandwidth. As seen in equation (2.15), by increasing the thickness of the crystal the nonlinear efficiency increase by the power of two. However, the sinc–function is at the same time limiting the bandwidth. The larger the thickness, L, the narrower the sinc-function will become, see figure 4. The results of the simulations for a thickness of 100 to 150 μm and an angle for θ between 22.5 and 23 degrees were evaluated and can be seen in the two following figures.

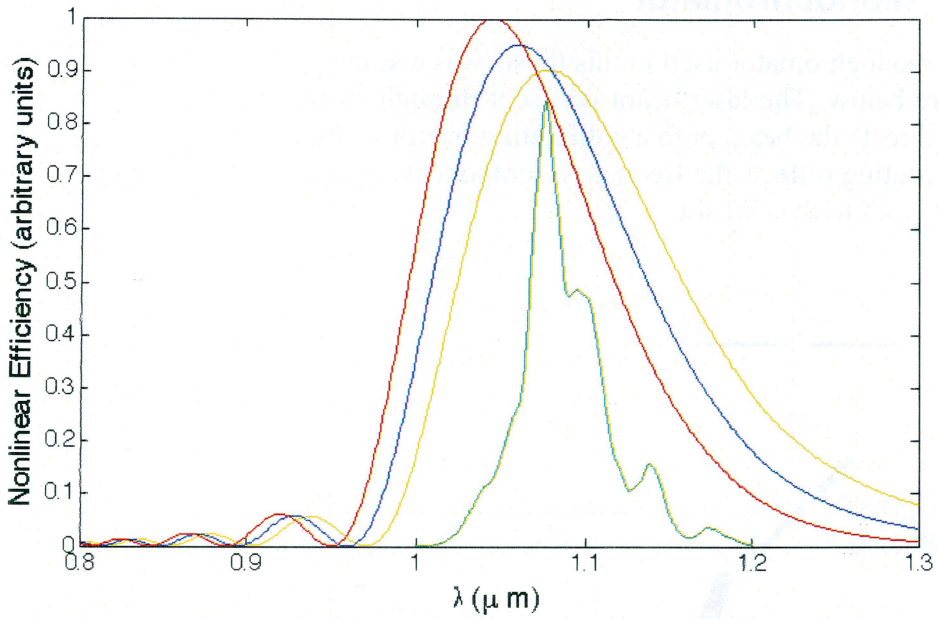

Figure 12. Nonlinear efficiencies with a crystal thickness of 150 μm for three different values for θ: 22.5°, the red curve, 22.75°, the blue curve, and 23.0°, the yellow curve. A spectrum of the laser, that is to be frequency doubled, has also been added.

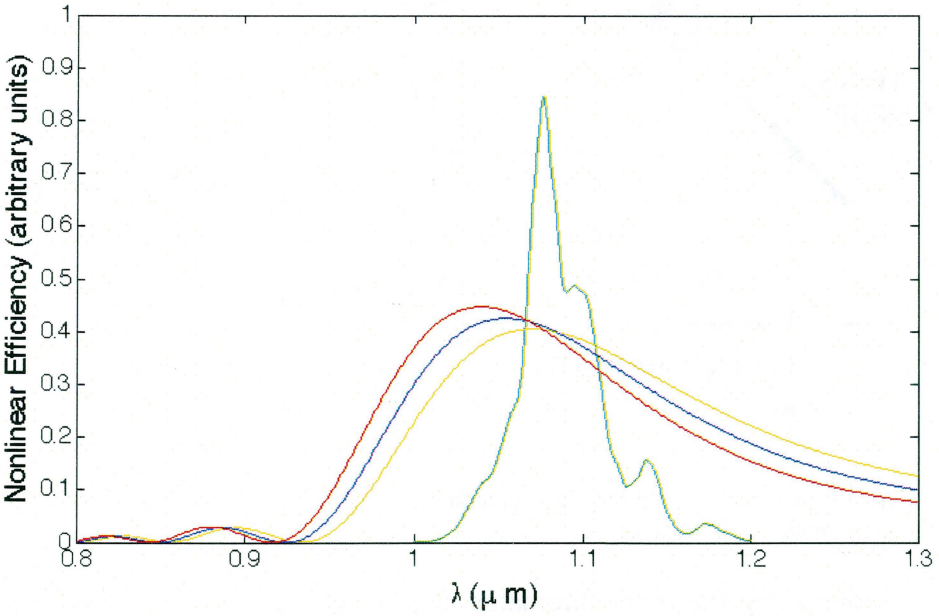

Figure 13. Nonlinear efficiencies with a crystal thickness of 100 μm for three different values for θ: 22.5°, the red curve, 22.75°, the blue curve and 23.0°, the yellow curve. A spectrum of the laser, that is to be frequency double, has also been added. The arbitrary units are the same as in figure 12 for comparison purposes.

As seen in the figures there would have been a more than doubled gain in the second harmonic generation if a crystal with the thickness of 150 μm had been used, but the bandwidth of the crystal was decided to be too small and we would get a far smother gain curve when choosing a crystal with thickness 100 μm. A BBO crystal of thickness 100 μm, angle θ with a value of 22.8° and the angle φ equal to 90° were chosen.

4.3 Monochromator

The monochromator used in this thesis was a scanning monochromator, as seen in the figure below. The laser beam was sent through an entrance slit onto a folding mirror that directs the beam onto a collimating mirror collimating the beam onto the grating. The grating reflects the frequency components selected by the grating over a focusing mirror out to the exit slit.

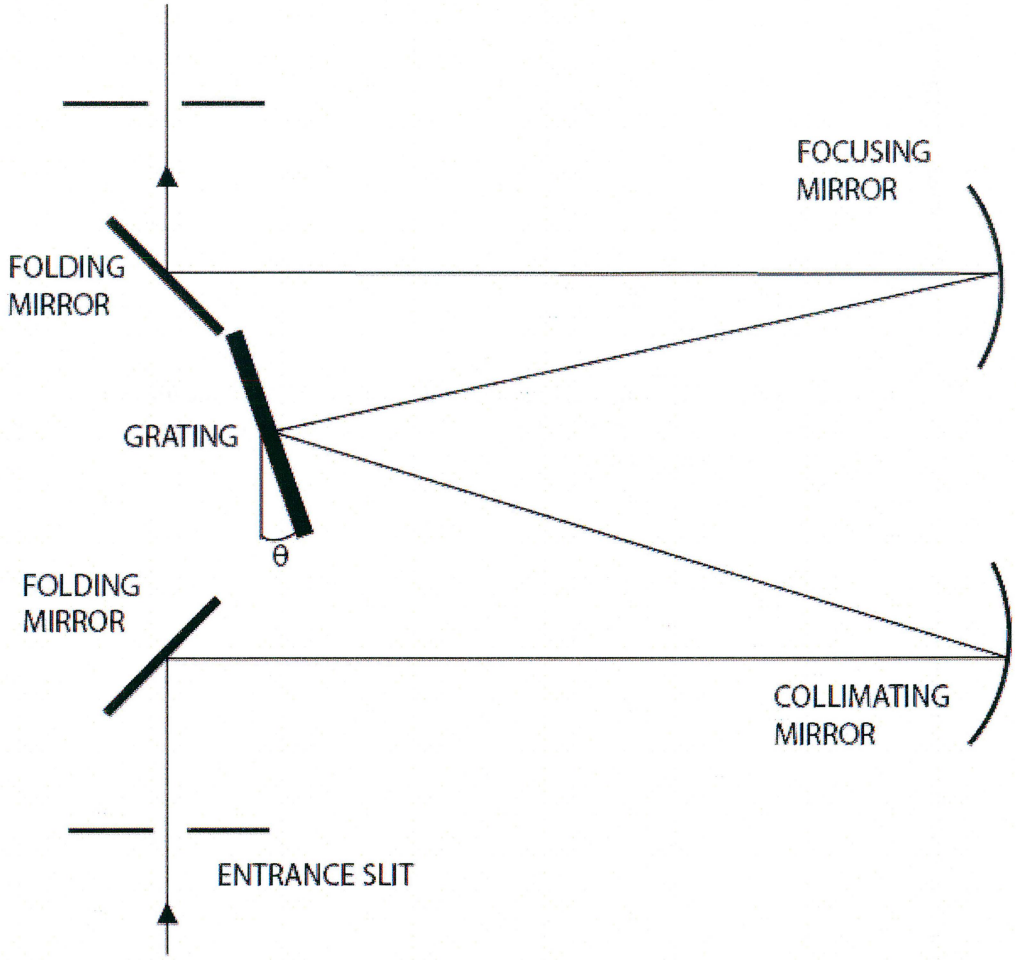

Figure 14. Schematics of the monochromator. Through the angle θ the wavelength that exits the monochromator can be chosen.

For controlling the monochromator, the General Purpose Interface Bus (GPIB) was used. Direct control could be made through a program, Measurement & Automation Explorer (MAX), on the computer or through programming a Labview program, see chapter 4.5, to do the communication automatically. The direct control was useful when setting up the FROG and for aligning the beam through the monochromator, but for actual measurements the Labview program was used.

4.3.1 Calibration of the Monochromator

A monochromator does not let every frequency through with the amplitude intact. It has a transfer function dependent on the wavelength. The reflection behavior of the grating and the spectral response of the photodiode vary between different wavelengths. First it had to be checked whether the monochromator had the right

calibration or not. This was done with a fluorescent lamp emitting light through excitation of mercury. The light of the lamp was sent through the monochromator and the mercury lines in the spectrum were identified. As the monochromator showed perfect agreement with the real position of the lines, no further wavelength calibration was needed.

To measure the transfer function a 'Globar', a glowing bar of SiliconCarbide (SiC) heated up to around 1300 K was used. The light of the Globar was sent through the monochromator and recorded by a detector. We were thus measuring the transfer function of both the monochromator and the detector. The Globar is known to send out radiation similar to a blackbody radiator radiating at around 1300 K. This was assumed to be the case, and the measured spectra from the monochromator and the lock-in detector were compared with the theoretical radiation from a black body radiator. The equation of a blackbody radiator looks as follows:

$$I(\nu) = \frac{2h\nu^3}{c^2}\frac{1}{e^{\frac{h\nu}{kT}}-1} \propto \frac{1}{\lambda^3\left(e^{\frac{h}{\lambda kT}}-1\right)} \tag{4.3}$$

The calculated transfer function was applied to a measured spectrum of the 1.07 μm laser pulse. The laser pulse had been measured with both the monochromator and detector and with a different spectrometer that had already been calibrated.

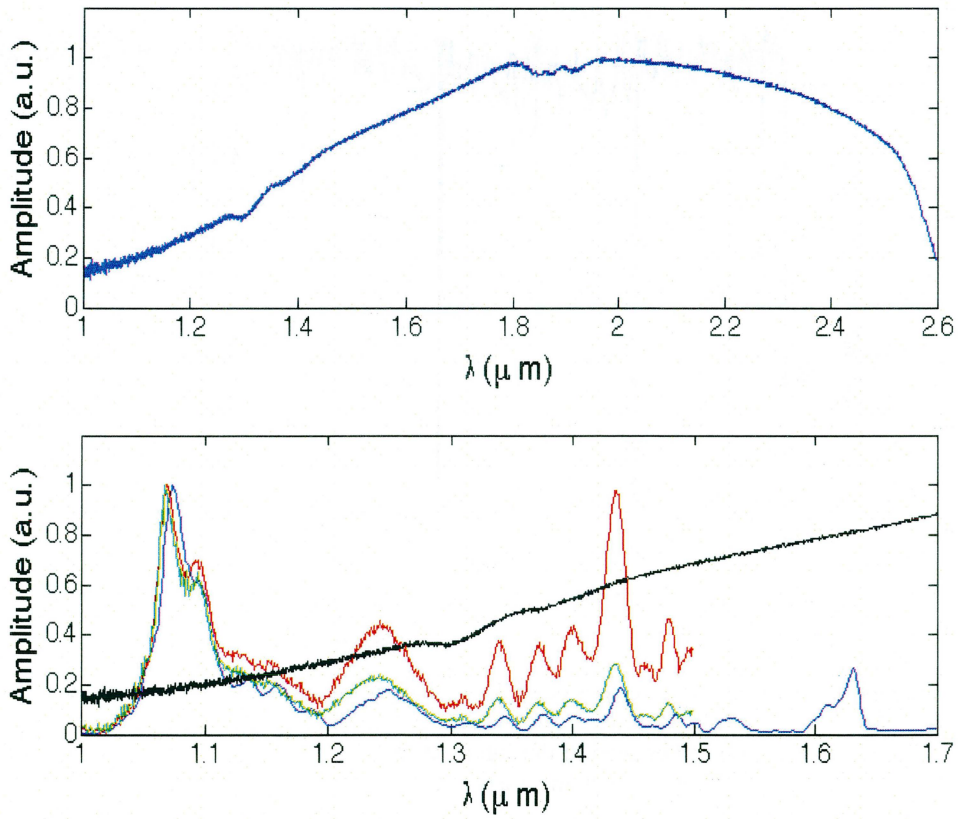

Figure 15. The upper part of the figure shows the entire response curve for the monochromator with detector. The lower part shows the spectrum of the laser measured with an already calibrated detector in blue. The red spectrum is the spectrum measured by the monochromator with detector. The black curve is the response curve from the figure above and the green spectrum is the spectrum measured by the monochromator divided by the response curve.

The spectrum measured by the monochromator divided by the response curve shows good agreement with the spectrum measured with an already calibrated spectrometer. The Globar's temperature was only assumed to be around 1300 K. What the real temperature was is not feasible to measure, but the assumption of 1300 K gave a good fit, as can be seen in the figure, and was thus used as a calibration curve for the rest of the thesis.

4.4 Stepper Motor and Controller

Both the stepper motor and controller used came from the same company, Newport. The stepper motor (UE16PP) had a resolution of 74 nm. The controller (MM4005) and controller card were put together to fit the stepper motor.

4.4.1 Calibration of Stepper Motor and Controller

The step distance of the stepper motor needed to be measured as it could possibly be vary sinusoidally over a few steps. By setting up a Michelson interferometer and measuring the fringes intensity as the stepper moved step by step, the step size could be evaluated. The results shown in the figure below were calculated by fitting a sinus function through the recorded intensity from the interferometer. The period of the extracted sinus-function is the double step length.

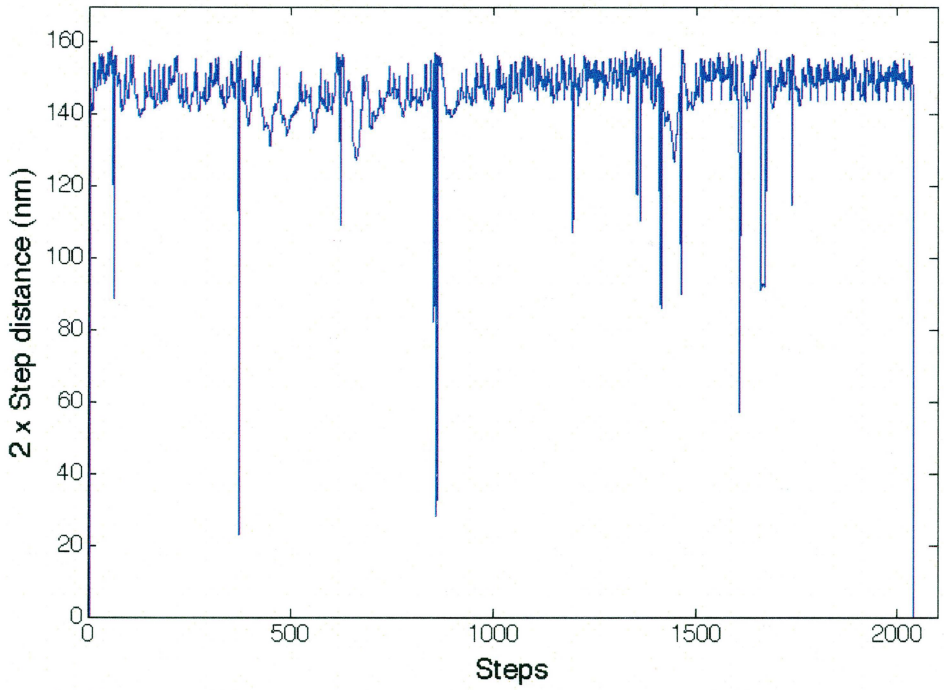

Figure 16. The steps from 0 to around 2000 were evaluated. The figure shows the step size twice as the real value as the laser has to travel twice the distance of every step in a Michelson interferometer. The spikes seen in the figure are artifacts from the algorithm used to calculate the step distance or possibly noise in the measurement caused by vibrations.

By measuring the distance the stepper motor moved when traveling from one end point to another with a precision instrument, a step size of around 74 nm was confirmed. This leads to a step size in the measurement of 148 nm (the path length is twice the length of the step length in a FROG setup) corresponding to a delay step in

the FROG setup of 0.5 fs. Such a small delay increment was more than enough for the FROG measurements that had step sizes of several femtoseconds up to picoseconds.

4.5 Spectrometer Recording Software

To control both the monochromator and the stepper motor to be able to measure a FROG trace, a program was written in Labview. For controlling the monochromator and being able to readout the measured data, a timed loop was used, starting with the command SCAN, see Appendix A, being sent to the monochromator and reading out values until the scan had finished. After every scan, a command was sent to the stepper motor to move one step forward, and a new scan was started. That way, spectrum after spectrum were recorded and were put together to produce a FROG trace. Common commands for the monochromator and stepper motor can be found in Appendix A: Device Programming.

4.6 Second Harmonic Generation FROG Retrieval

For a SHG FROG, a spectrally resolved autocorrelation is measured, as explained in chapter 2.2. A spectrum is recorded for every delay point.

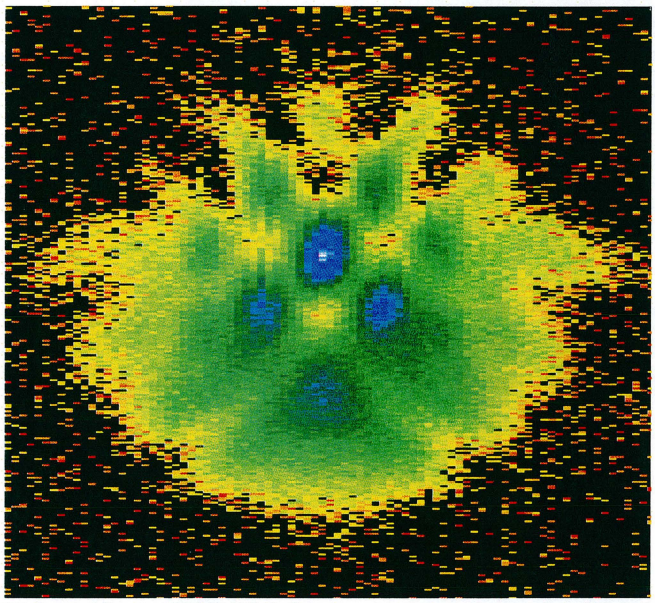

Figure 17. A SHG-FROG trace measured by the FROG setup built within this thesis. The spectrums of the different delay points have been measured and added together to create the SHG-FROG trace. Frequencies are shown on the y-axis and the delay points on the x-axis.

After measuring a SHG-FROG trace, one has to retrieve the original pulse. This is done through several steps of iteration until a predetermined parameter, typically the error of the iteration, has reached an acceptable value, or by manual termination of the iteration.

4.6.1 Pulse retrieval algorithms

There exists several different FROG retrieval algorithms, but they all use the same form for the FROG error, G, as:

$$G = \sqrt{\frac{1}{N^2}\sum_{i,j=1}^{N}\left|I_{FROG}(\omega_i,\tau_j) - \alpha I_{MEASURED}(\omega_i,\tau_j)\right|^2}\ , \tag{4.4}$$

where N is the size of the grid of the FROG trace[2], I_{FROG} the intensity of the reconstructed FROG trace, $I_{MEASURED}$ is the measured intensity of the FROG trace and α is a scaling factor which is chosen to minimize G, the FROG error. The error depends on the grid size N of the FROG trace, on the noise and on the grid size actually covered by the signal. Thus, it is difficult to use the FROG error for comparing different measured FROG traces, but it can still be used as an indication whether the FROG retrieval produced a result close to the original signal or not.

Because of its simplicity one of the first algorithms to be used, and one of the fastest in terms of time per iteration, was the basic FROG algorithm[15]. The algorithm starts with a guess for the electric field, E(t). The guess can be manually chosen to be either pure noise, intensity noise or phase noise[3]. As no difference in the result of the FROG retrieval was observed between the initial guesses, the default (phase noise) was chosen. From this first guess a signal field is calculated:

$$E_{sig}(t,\tau) = E(t)E(t-\tau) \tag{4.5}$$

After a fast Fourier transform (FFT) and by squaring the signal field, one arrives at the FROG trace, $E_{sig}(\omega,\tau)^2$. The next step in the iteration is applying the measured FROG trace to the calculated trace as follows:

$$E'_{sig}(\omega,\tau) = \frac{E_{sig}(\omega,\tau)}{\left|E_{sig}(\omega,\tau)\right|}\sqrt{I_{MEASURED}(\omega,\tau)} \tag{4.6}$$

The new signal field is transferred back into the time domain by an inverse fast Fourier transform (IFFT). Through integration of the signal field in the time domain along the delay axis, one arrives back at the electric field E(t) and a new iteration can be started.

[2] The FROG-retrieval program interpolates the points of the measured FROG trace to match a matrix with NxN pixels.

[3] The intensity of the initial guess is a Guassian with random phase noise.

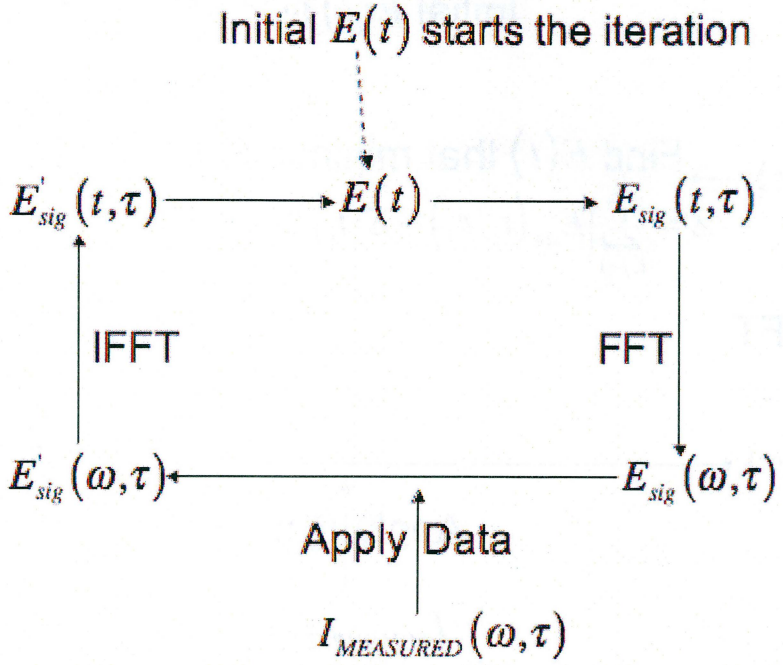

Figure 18. Schematics of the basic FROG algorithm. The initial guess of the electric field starts the iteration and at the end of the iteration a new electric field is calculated and the loop continues. FFT stands for fast Fourier transformation and IFFT for inverse fast Fourier transformation.

As the basic FROG algorithm suffered from drawbacks[16], such as slow conversion for FROG traces with high complexity, a newer, more powerful, method was developed. The algorithm using generalized projections[17] projects the guess of the FROG trace on two sub-spaces; the measured FROG trace and the mathematical form of the signal field, see equation (4.5).

The projections are made between the two sub-spaces trying to find a solution that satisfies both constrains. This solution would be the exact reconstruction of the FROG trace.

The main difference between the basic FROG algorithm and the generalized projections algorithm is that while the basic FROG algorithm, through integration of the signal field in the time domain along the delay axis, arrives back at the electric field E(t) the general projections algorithm tries to find an electric field that minimizes the error metric, Z.

$$Z = \sum_{i,j=1}^{N} \left| E'_{sig}(t_i,\tau_j) - E(t_i)E(t_i-\tau_j) \right|^2 \qquad (4.7)$$

The schematic of the generalized projections algorithm looks as follows:

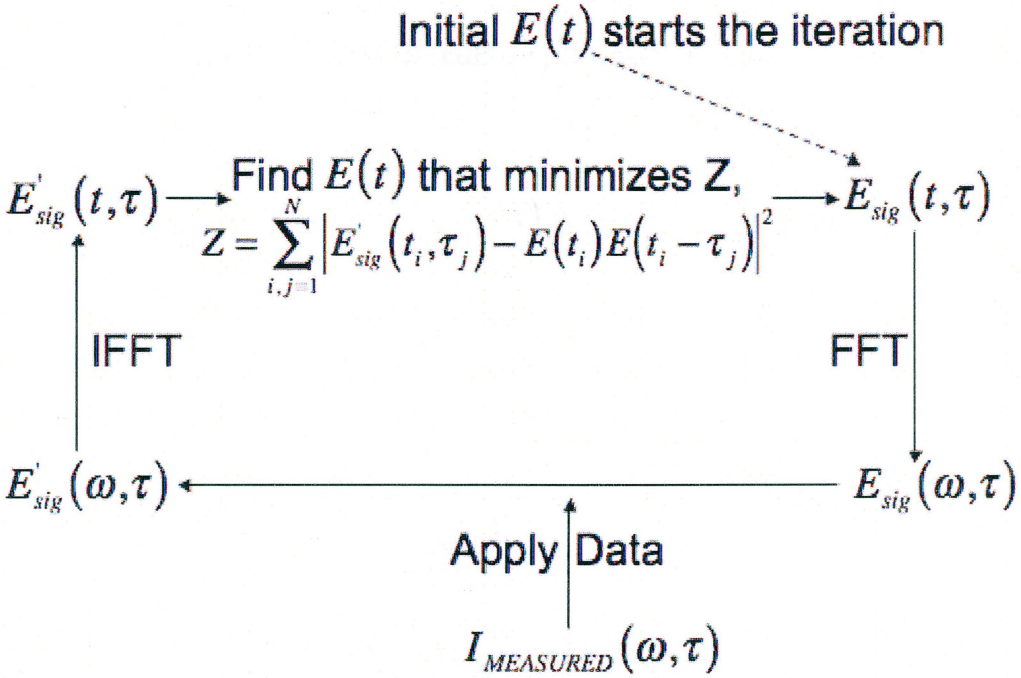

Figure 19. The schematic for the generalized projections algorithm. The initial guess of the electric field starts the iteration and at the end of the iteration a new electric field is calculated through minimization of the error metric, Z, and the loop continues. FFT stands for fast Fourier transformation and IFFT for inverse fast Fourier transformation.

4.6.2 Trivial and Nontrivial Ambiguities with FROG

As stated in the previous chapter: that the FROG algorithm converges to one value alone is not entirely true. There exists some nontrivial ambiguities[18] with the FROG algorithm. A few of the more trivial ambiguities is that it has been shown that the electric field E gives the same FROG trace as $E \times \exp(ia)$.

E(t) also gives the same FROG trace as E(-t) which corresponds to E(ω) giving the same FROG trace as E*(ω) in the frequency domain. The reason for this is the FROG measurements being center symmetric. All information about what pulse comes before the other one (or which way the gate arm is being moved) is lost.

This gives a problem when trying to determine the GDD of the pulse. As we don't know whether we have reconstructed the pulse E(ω) or E*(ω), we can not know whether the reconstructed phase has got a negative or positive sign. There are ways of solving this issue. One can of course know the GDD and thus easily determine which of the two possible FROG traces that was reconstructed, or one can introduce a change in the GDD by measuring two FROG traces of the same laser with a piece of glass in between during one of the measurements. One can calculate if the GDD added should be positive or negative. If the GDD added is calculated to be positive and the GDD in the retrieved FROG trace with the slab of glass in between becomes stronger (more curvature) then the GDD of the first measurement must have been already positive, we only added more GDD. If the curvature decreases, the GDD was originally negative.

One last way of determining which pulse you retrieved is by inserting a thin piece of glass in the beam path, thus producing multiple reflections which will trail behind the real pulse into the detector. If the reconstructed FROG trace shows a trail of

several smaller pulses before the main pulse the FROG trace with the inverse time dependence, E(-t), must have been retrieved by the algorithm.

A nontrivial ambiguity arises from the fact that as a SHG-FROG trace is produced by two identical pulses it must always be center symmetric. It has however been proven that two different pulses can create center symmetrical FROG traces[18]. A symmetrical FROG trace is thus no guarantee for two identical pulses. This may occur when the beamsplitters have not been properly optimized giving rise to spectral shaping and phase filtering. Even though it is a nontrivial ambiguity, and cannot easily be checked, one has to assume that several different measurements of the same laser over a period of time must be correctly reconstructed if they give a consistent answer.

4.7 FROG Retrieval Program

Once the FROG trace has been read in correctly, see Appendix B: File Formats, there are several ways to modify it before starting the retrieval. If a selection of the data has been overcome by noise it can be deselected by selecting the parts of the trace still useable.

There exist four different methods for reducing the noise in the measured FROG trace.

1. Full Spectrum: The average of the two spectra at each end of the FROG trace (the spectra with the smallest and largest time delay) is subtracted from the entire FROG trace as there should be no real signal there. By doing so any stray light entering the monochromator will be subtracted as is not affected by the delay points and therefore can be found at the edges of the traces as well as at the centre.

2. Lowest Pixel: By subtracting the value of the lowest pixel from the entire trace any noise, such as dark current, can be removed. This is to be preferred instead of the full spectrum in case the signal got truncated at the edges of the trace as a full spectrum removal would remove some of the signal.

3. Edge: The 'Edge' mode takes the average of the two rows of pixels closest to the border all around the trace and subtracts it from the spectrum. Once again, if the measurement was not truncated at the edges this should only remove noise.

4. Fourier Low Pass: The FROG trace is Fourier transformed into the frequency space and low pass filter, a circular Gaussian filter, is multiplied with the FFT of the FROG trace. This smoothes the FROG trace.

The FROG retrieval program uses fast Fourier transforms to transform the trace between time and frequency space. The measured FROG trace has to be fitted to a grid that satisfies the Fourier relationship between time and frequency. This means that the delay and the frequency axes of the trace are related to one another through a Fourier transform relationship.

$$t = \frac{2\pi}{\Omega} \tag{4.8}$$

$$T = \frac{2\pi}{\omega} \tag{4.9}$$

Here t is the delay increment, T the total delay range, ω the wavelength increment and Ω the wavelength range. When using a larger than normal delay range a higher than normal spectral resolution of the measured spectra must be used, i.e. a smaller wavelength increment is needed. If the spectrometer is not capable of such fine resolution a new spectrometer, or interpolating the values to a high enough resolution, is needed.

5 Results

When measuring the laser at frequency 1.07 μm it was quickly noticed that the low power of the laser led to noisy FROG traces. Furthermore, the long beam path of the laser led to instabilities and errors in the traces. With many mirrors and a lot of air between the seed laser and the FROG setup, there are many possible sources of noise. Because of vibrations disturbing the mirrors, or a change of refractive index in the air caused by airflow, slight alterations to the beam path of the laser can occur. There was still the issue of a long beam path for measurements on the 3.6 μm, but the instabilities of the laser gave the largest error in the FROG traces and were what was limiting the resolution of the FROG traces obtained throughout this thesis. The first successful FROG trace measured can be seen below.

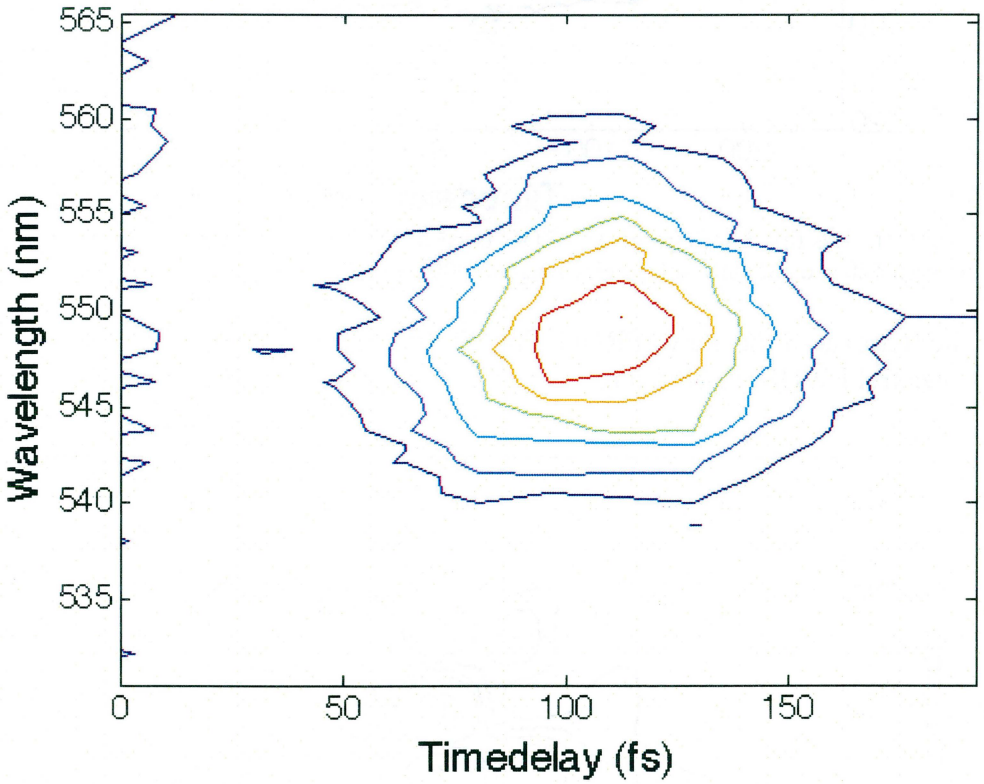

Figure 20. The first FROG trace recorded. The leftmost spectrum shows some noise which can be removed by selecting the part to the right of it in the FROG program.

The highest resolution of a FROG traces was obtained when measuring the 1.07 μm overnight to minimize outside influences, such as vibrations, and can be seen below.

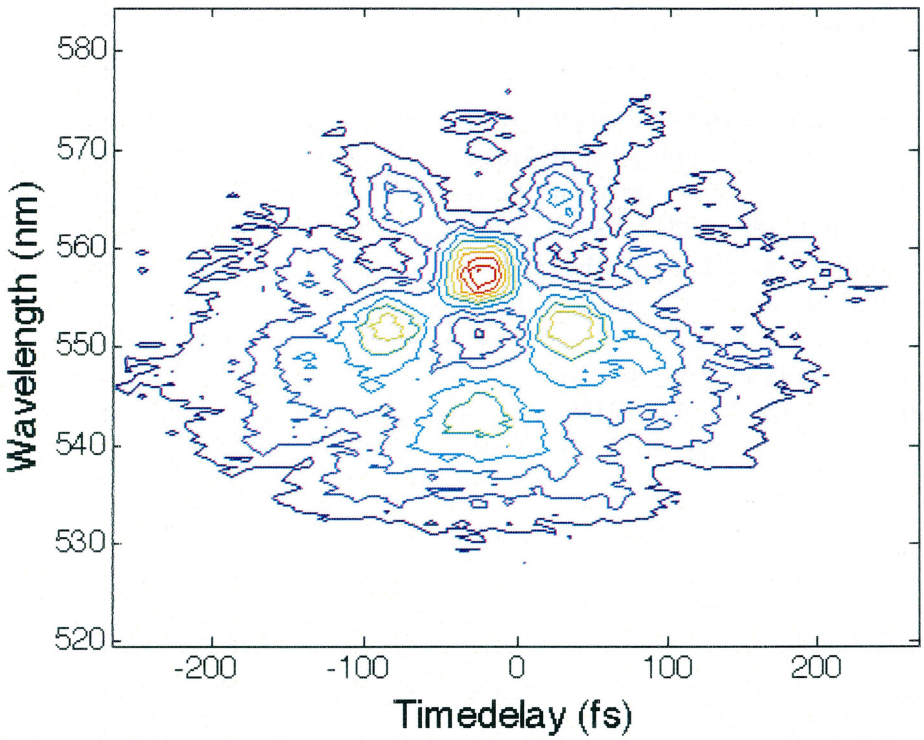

Figure 21. The first highly resolved FROG trace of the 1.07 μm laser. Wavelengths captured between 520 and 585 nm, with a delay range of 500 fs.

The retrieval of the above FROG, Fig. 22, trace gave a temporal FWHM of 146 fs and a spectral FWHM of 38.4 nm.

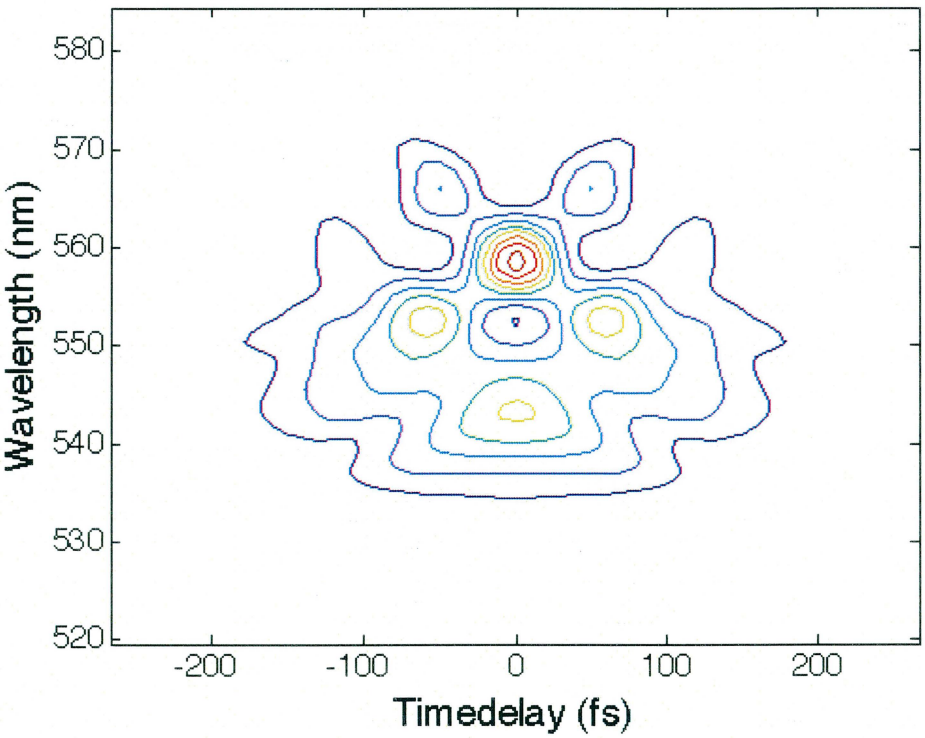

Figure 22. The reconstructed FROG trace of the previously shown FROG trace (see figure 21). The retrieved trace had a temporal FWHM of 146 fs and a spectral FWHM of 38.4 nm.

While measuring there was the issue with the laser being sensitive to outside influences such as vibrations in the optical table and airflow. A door opening could easily ruin a measurement. Opening the door causes the spectrum of the FROG traces to shift temporarily. This lead to single, or more, spectra in the FROG trace being distorted, which can be seen in figure 23.

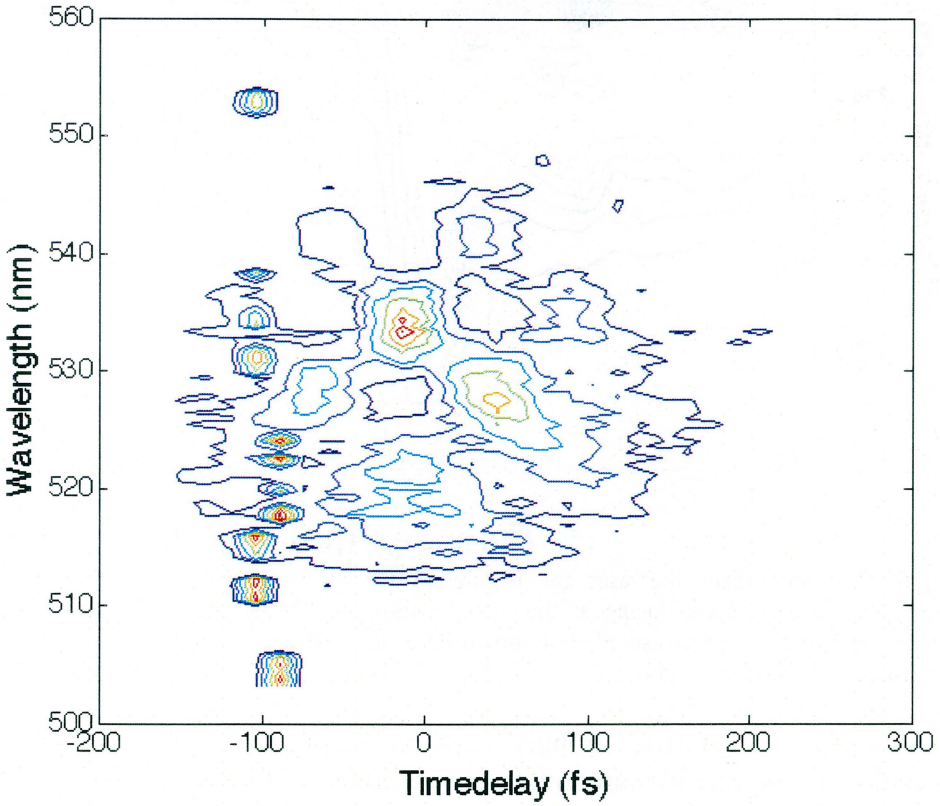

Figure 23. The door to the lab was opened during the measurement, which can be seen in the left of the trace. This trace can not be used for the FROG retrieval algorithm.

The disturbances, as seen in the above figure, can cause artifacts in the measured traces that will ruin any FROG retrieval attempts.

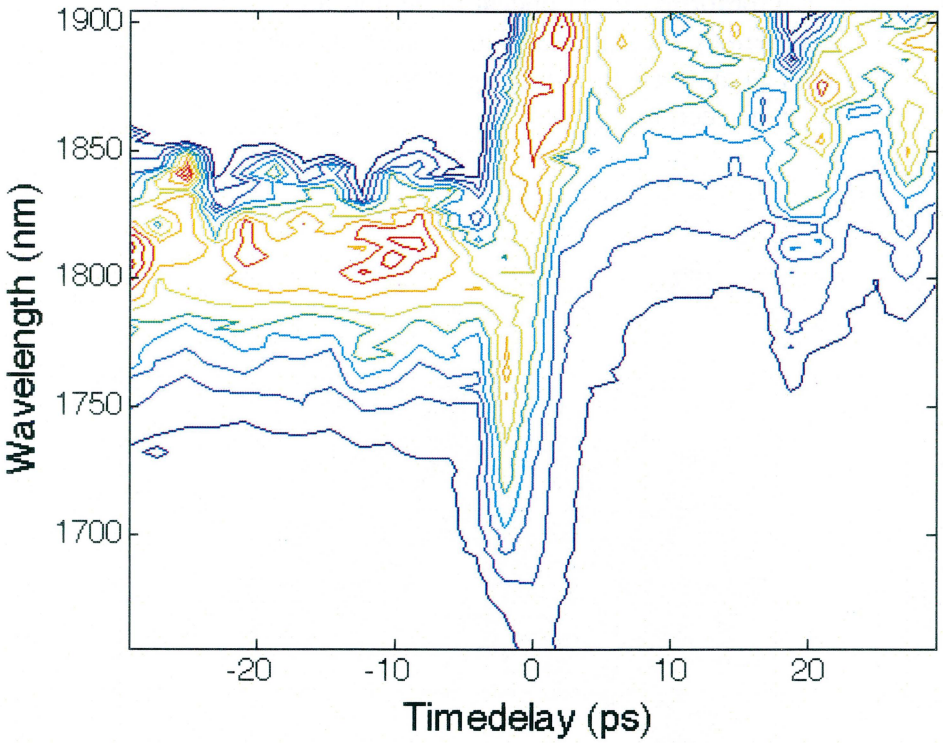

Figure 24. Once again, the laser got misaligned due to outside influences. The laser made a sudden jump and stayed lasing at the new 'position' in the spectrum for some time. In the following FROG trace measured (not shown here) the laser had jumped back to normal lasing with a normal spectrum again.

As the noise level rose strongly with people present in the lab, scans were conducted when no one was around; over lunchtime, at night and over the weekend. This lowered the noise in the scans noticeably. But that led to a new issue: Because the monochromator is a scanning monochromator, it scans through the entire spectrum instead of reading it out all at once as a spectrometer would. Therefore, it takes time to measure a spectrum. Consequently, the scan times that were required to obtain a decent resolution on the FROG trace were very long. Scans of 30 minutes or more were needed for the measurements at 3.6 μm. Because of the long scan times the drift of the laser became a problem. The laser would slowly loose power over a period of time and a recalibration of the laser was necessary. The laser would also make spontaneous jumps in the spectrum, jumping back again after a few minutes. The solution to this was easy, but time consuming: FROG traces were measured repeatedly until a decent trace could be recorded.

A different kind of problem that could arise with the measured FROG traces occurred when the directly generated second harmonics were not blocked properly. When this was the case, a second harmonic signal was visible independently of the delay position.

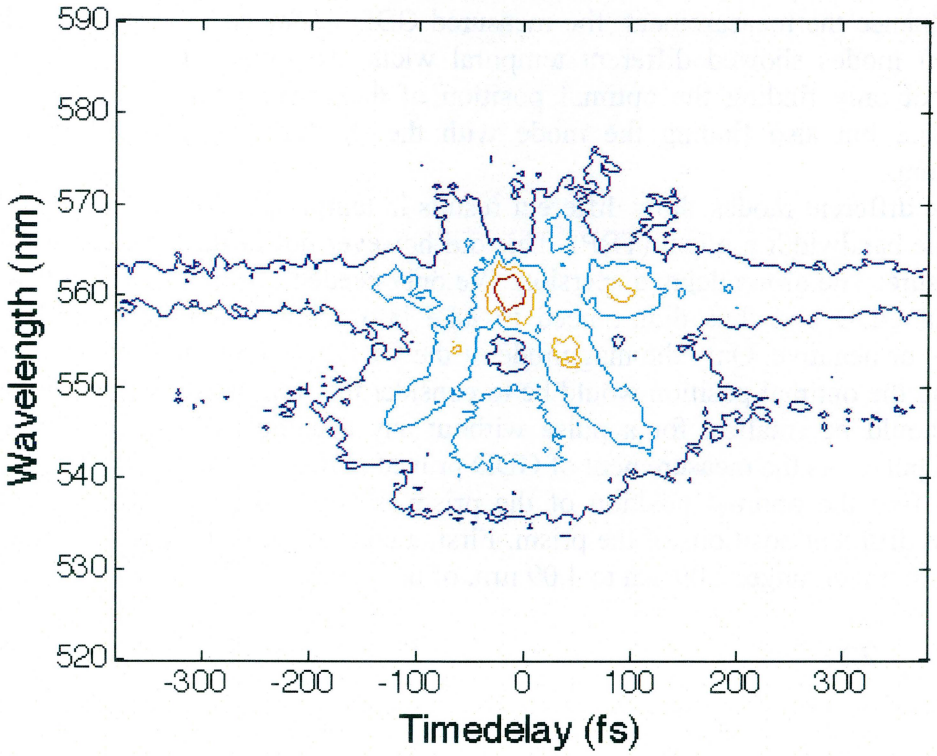

Figure 25. The directly generated second harmonic was not blocked of properly and can be seen as wings of the FROG trace.

As can be seen in figure 25, failing to block the directly generated second harmonic light caused wings to appear on the FROG trace. This can be easily removed by using the Frog program. By using the noise reduction scheme 'Full Spectrum' as described in section 4.7, an average of the spectrum at the side of the FROG trace is removed from the entire trace, thus removing the wings.

5.1 Results of Positioning of Prism in the Laser Setup

When generating the white light continuum from the highly nonlinear fiber, HNLF, see chapter 3, figure 8, two prisms together with a knife edge are used for choosing what frequencies are picked from the generated white light and for recompression of the fiber output. By moving the knife edge into the beam, after it has been split up in its frequency parts by the first prism, one can control which frequencies are let through to the difference frequency generation, DFG, thereby choosing the frequencies that will be generated. By moving one of the prisms in and out of the beam, nothing will change with the selected frequencies, but more or less material will be put into the path of the beam. A laser beam passing through a material will gain some GDD. As the laser was designed to produce as short laser pulses as possible, a pulse without any GDD is needed. To try to minimize the GDD with the help of the prism, the FROG setup was designed to work around the frequency 1.07 μm. Beamsplitters and a nonlinear crystal were chosen to fit this purpose. After passing over the prism, the generated white light from the HNLF was sent into the FROG and recorded. Trying to find the position with the minimal GDD, several different FROG traces were recorded at different positions for the prism.

As the determination of the optimal position of the prism took more than one day, a recalibration of the laser took place in-between the measurements. This led to a

change in the frequency output of the fiber. The change of the emitted spectrum did not influence the measurement, the measured GDD remained the same, but the two different modes showed different temporal width. To obtain the shortest possible pulse not only finding the optimal position of the prism giving minimal GDD is important, but also finding the mode with the shortest temporal full width half maximum.

The different modes show different results in temporal FWHM, spectral FWHM and time bandwidth product (TBP). This did however not influence what we wanted to measure: The group delay dispersion. We only needed to find the position with the minimal GDD and thus didn't need to take into account whether the GDD was positive or negative. Only the magnitude of the GDD was important. Another way of deciding the optimal position would be to consider the time bandwidth product, TBP, as it should be smallest for a pulse without any accumulated GDD, a bandwidth limited pulse. As the measurement of GDD proved sufficient, this was not needed.

To find the optimal position of the prism, several FROG measurements were made at different positions of the prism. First, a coarser measurement was made over the entire travel range, 2.09 μm to 4.09 μm, of the prism.

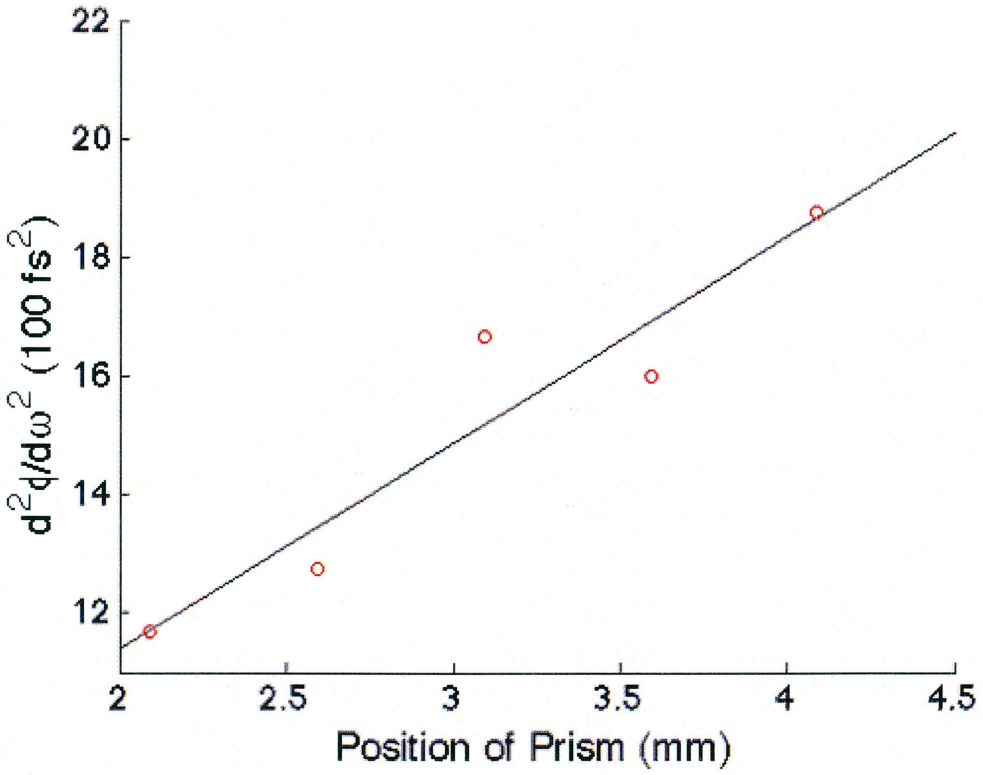

Figure 26. The measured GDD of the positions of the prism. A line has been fitted through the measured data to emphasize the linear trend.

Position	TBP	GDD (100 fs^2)
2.09	1.14	11.68
2.59	1.36	12.76
3.09	1.42	16.68
3.59	1.63	16.01
4.09	2.09	18.75

Table 3. Time bandwidth product and the measured GDD for five different positions over the entire travel range of the prism as seen in figure 26.

As can be seen in table 3, the GDD and the time bandwidth product indicates that the position for minimum GDD might be outside of the travel range or at least very close to the travel limit. The recorded FROG trace and the reconstructed spectrum and phase can be seen in the following figures.

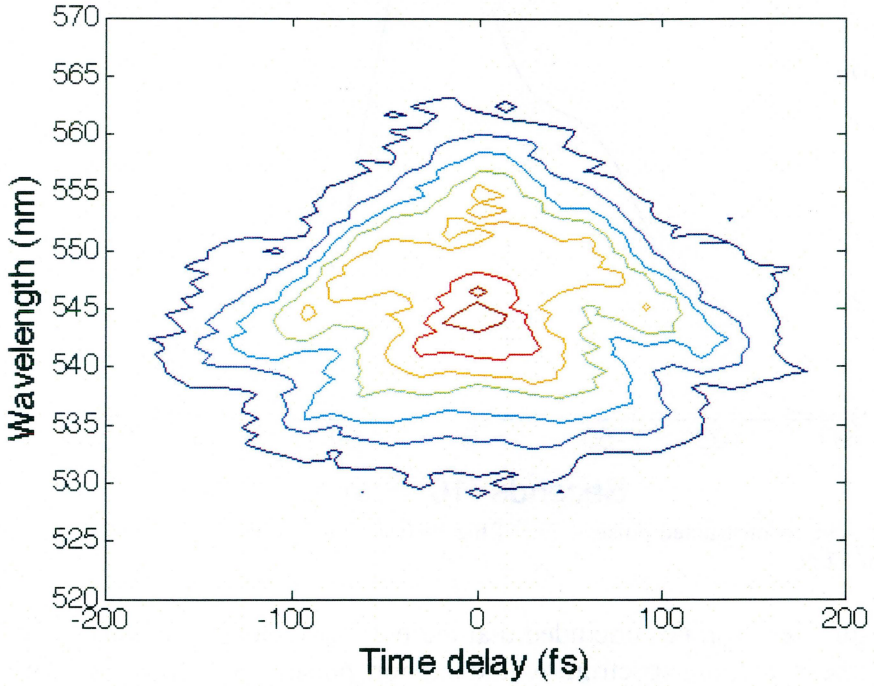

Figure 27. FROG trace recorded with the prism at position 2.09.

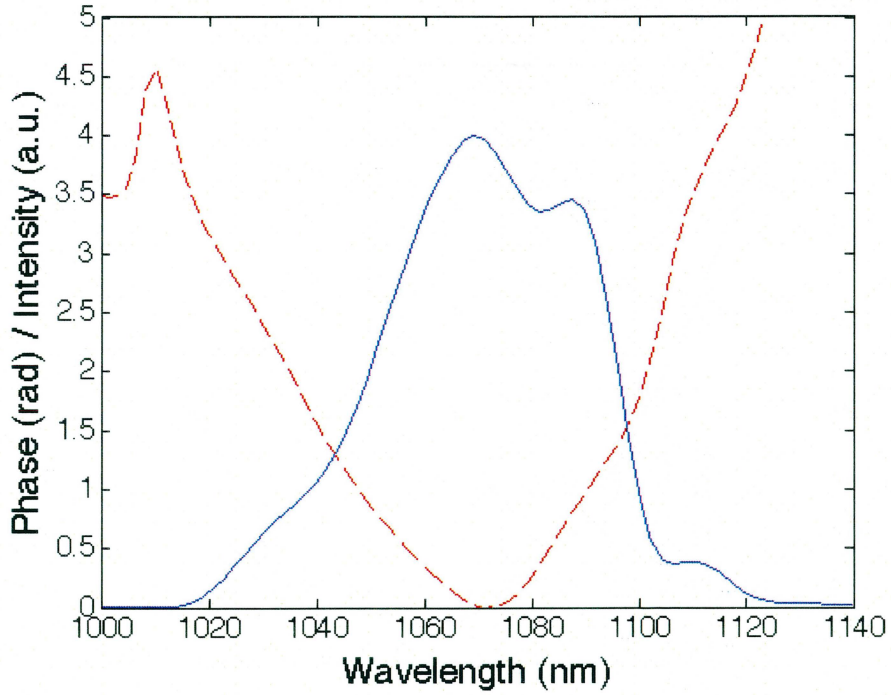

Figure 28. The reconstructed spectrum (blue line) and the reconstructed phase (red line) from the FROG trace recorded at position 2.09 with the prism. The phase shows the GDD calculated to be 1168 fs^2. The arbitrary units of the spectrum have been fitted to the maximum of the phase.

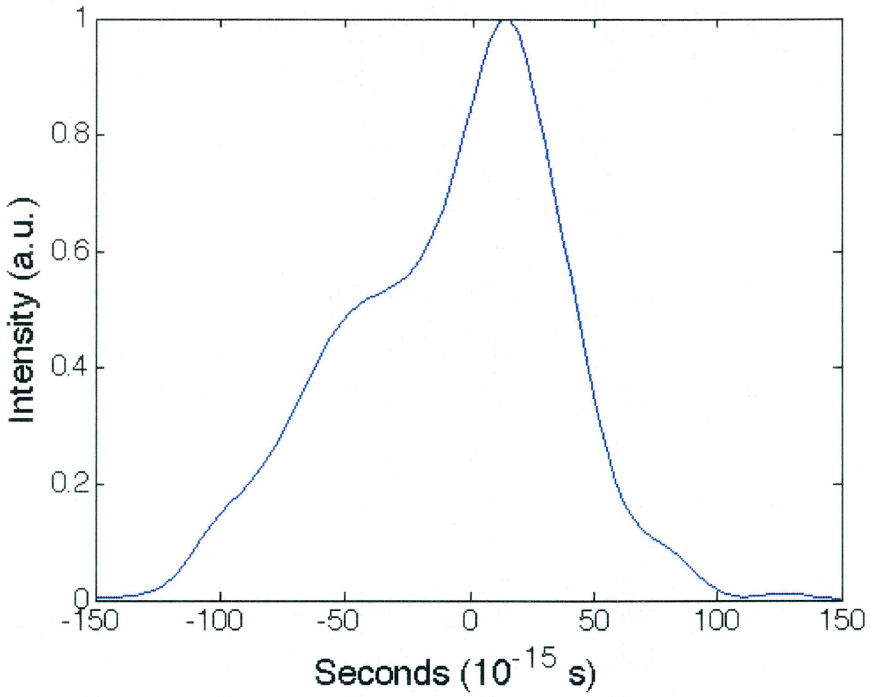

Figure 29. The reconstructed pulse shape of the FROG trace visible in figure 28 with a temporal FWHM of 82 fs.

From figure 28 it can be concluded that there exists GDD in the pulse. If the GDD could be compensated, the spectrum would support pulses down to 32 fs. How strong the GDD is can be calculated by fitting a second degree polynomial through it and taking the second derivative thereof.

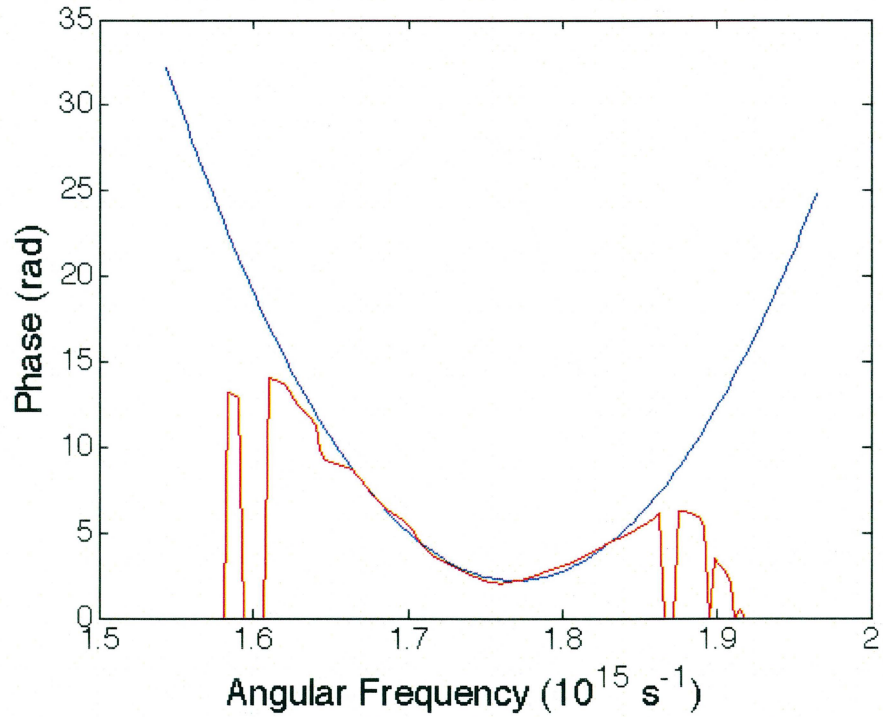

Figure 29. To extract the GDD of a retrieved pulse, a second degree polynomial, blue line, was fitted to the phase, red line. The second derivation of the polynomial gave the GDD. The GDD of the phase in the above figure was calculated to be 1168 fs^2.

To double check the measurements made of the GDD at the different positions of the prism, a new measurement was made a few days later. Here, the mode in which the laser was lasing had changed and the time bandwidth product changed with it. But as can be concluded from table 4, the GDD did not.

Position	TBP	GDD (100 fs^2)
2.1	2.39	11.70
2.2	2.23	12.95
2.25	2.34	13.01
2.3	2.3	13.48
2.8	2.7	13.38

Table 4. Time bandwidth product and the recreated GDD for five different positions close to the travel limit of the prism. An extra measurement at position 2.8 was taken to be able to double-check the results with the previous measurement. It becomes clear that the optimal position of the prism must exist outside the travel limit.

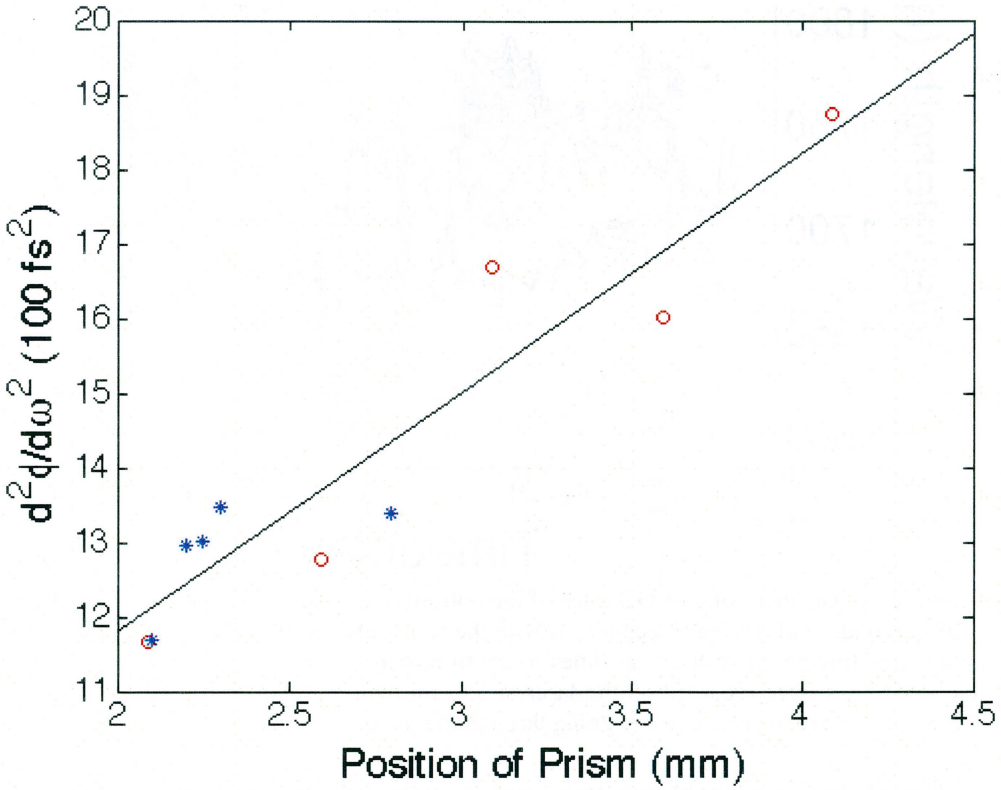

Figure 30. The measured GDD of the different positions of the prism. The earlier measurements are marked with red rings and the later with blue stars. A line has been fitted through the measured data to emphasize the linear trend. It is clear that the optimal position of the prism exists outside the travel range.

It was concluded that the optimal position must be outside the travel limit of the prism.

5.2 Results of Measurements on the Mid-Infrared Laser

When measuring the FROG trace of the laser in the mid-infrared, 3.6 μm, new beamsplitters and a new nonlinear crystal had to be installed. As the laser could only be seen with a thermally sensitive liquid crystal paper, a Helium-Neon (HeNe) laser was used for aligning the beam through the FROG setup. The liquid crystal was used

to superimpose the HeNe on the mid-infrared laser. As a result, the HeNe laser could be sent through the FROG setup and a lot of time consuming work using a power meter trying to localize and sending the mid-infrared laser through the FROG setup was avoided.

As it turned out, the laser in the mid-infrared was far more sensitive than the laser in the short-infrared range (1.07 μm). Vibrations caused the laser power to drop down to around zero and the laser had to be recalibrated. The laser also experienced longtime drifts reducing the output of the laser over time. Fast scans on an initially stable laser were needed.

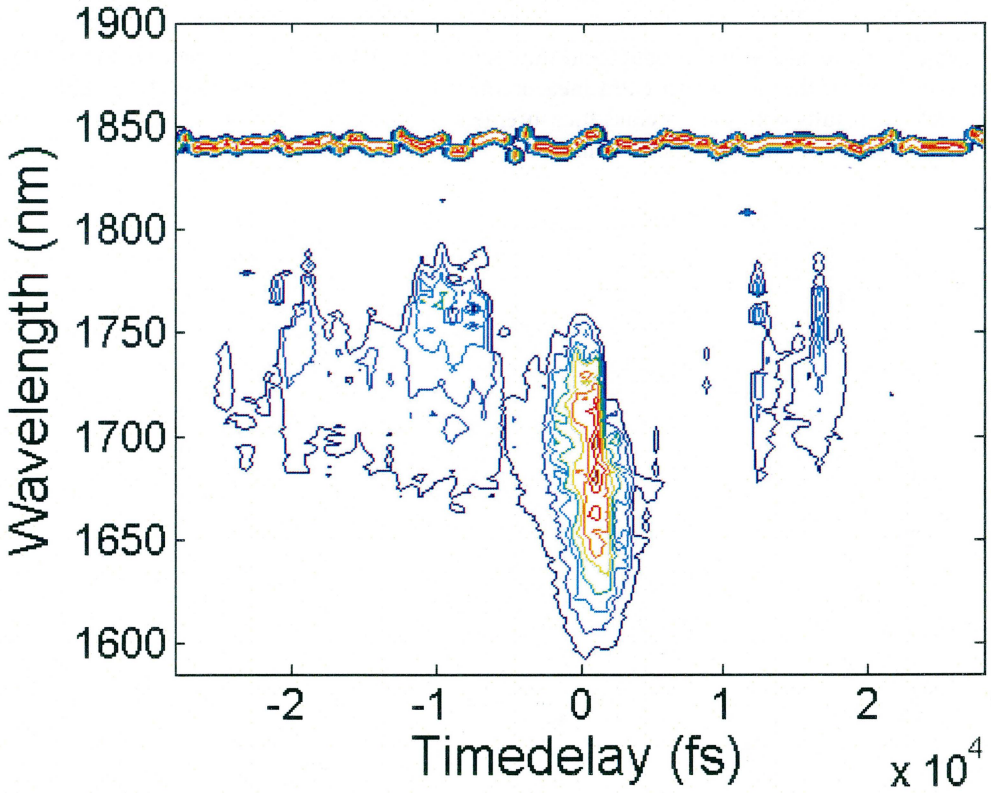

Figure 31. The measured FROG trace of the mid-infrared laser. Note the delay ranges over several picoseconds, and not femtoseconds, as with the short-infrared laser. Because of the instabilities of the laser forcing down the scan times to try to minimize the influence of the instabilities, much fewer points were recorded on the laser at 3.6 μm than at 1.07 μm. In the top of the figure the HeNe laser can be seen as a line going through the trace.

Several different problems arose when retrieving the original pulse with the Frog program. As said before, instabilities gave noisy traces which could be partially countered by removing the noise by hand. One of the recorded FROG traces of the mid-infrared laser was done with the directly generated second harmonics not being blocked totally. This was easily removed by the FROG retrieval program. But not only did the direct SH get through the monochromator, but also the third order of the HeNe laser, situated at 1900 nm, see upper part of figure 31, got through. In the figure, the HeNe is clearly seen at 1850 nm instead of 1900 nm. This is an effect of the HeNe laser not entering the monochromator at a perpendicular angle, thus exiting it at the "wrong" frequency. The HeNe was used to recalibrate the FROG trace as every spectrum got shifted between the different delay points due to issues with the monochromator. The trace was also far from center symmetric, an effect of the instabilities. This could be changed by folding the right side of the trace over the middle, thereby artificially creating a center symmetric trace.

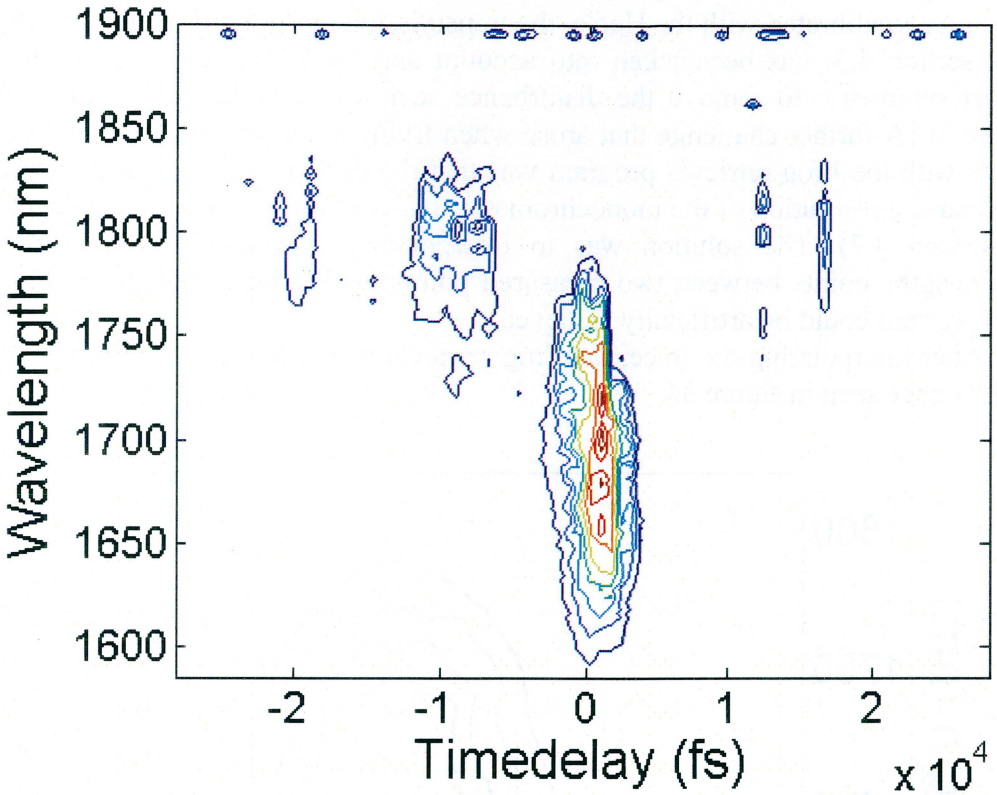

Figure 32. What the measured FROG traces looked like reducing some of the noise and recalibrating it with the help of the HeNe.

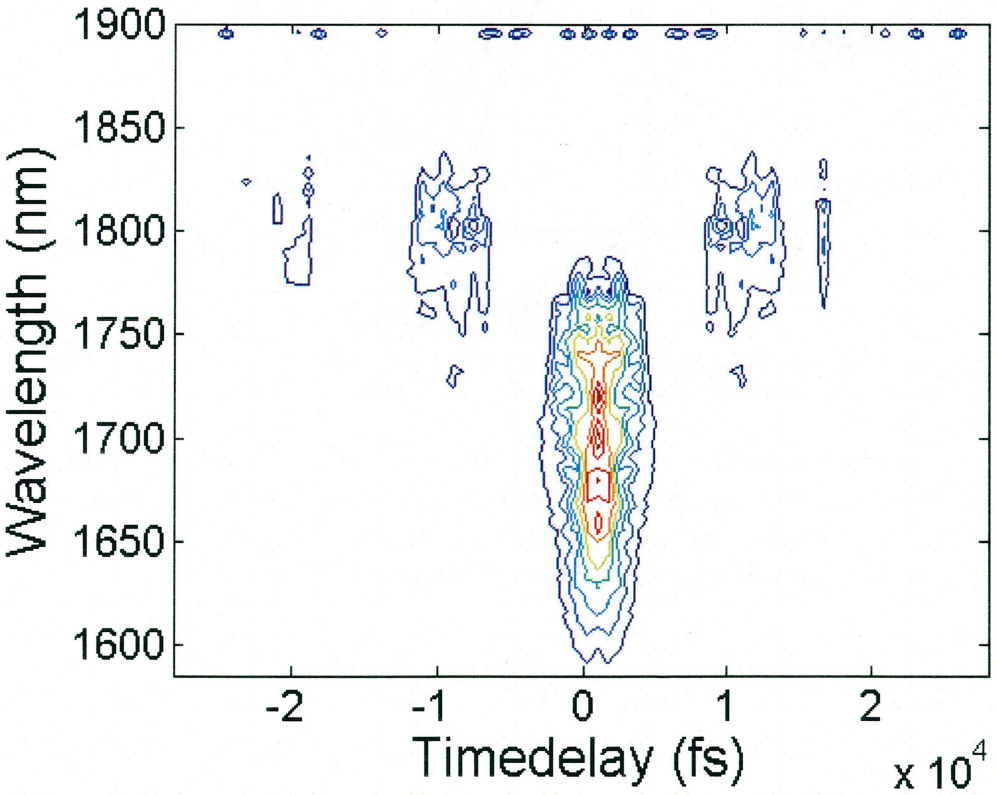

Figure 33. The FROG trace of figure 31 has been made center symmetric by folding the right side over the middle to remove the noise on the left side. The transmission function of the monochromator has also been taken into account.

In figure 33, the finished product is presented. The noise has been removed, every spectrum recalibrated with the HeNe, the transmission function of the monochromator (see section 4.3) has been taken into account and the FROG trace has been made center symmetric to remove the disturbance seen on the right side of the trace in figure 31. A further challenge that arose when trying to recreate the measured FROG traces with the Frog retrieval program was that the delay range, several picoseconds, demanded a resolution of the monochromator that could not be obtained (as explained in section 4.7). The solution was to interpolate the data, adding several more wavelengths points between two measured points, until a high enough resolution of the spectrum could be artificially achieved.

After interpolating the trace, the Frog retrieval program could finally retrieve the FROG trace seen in figure 34.

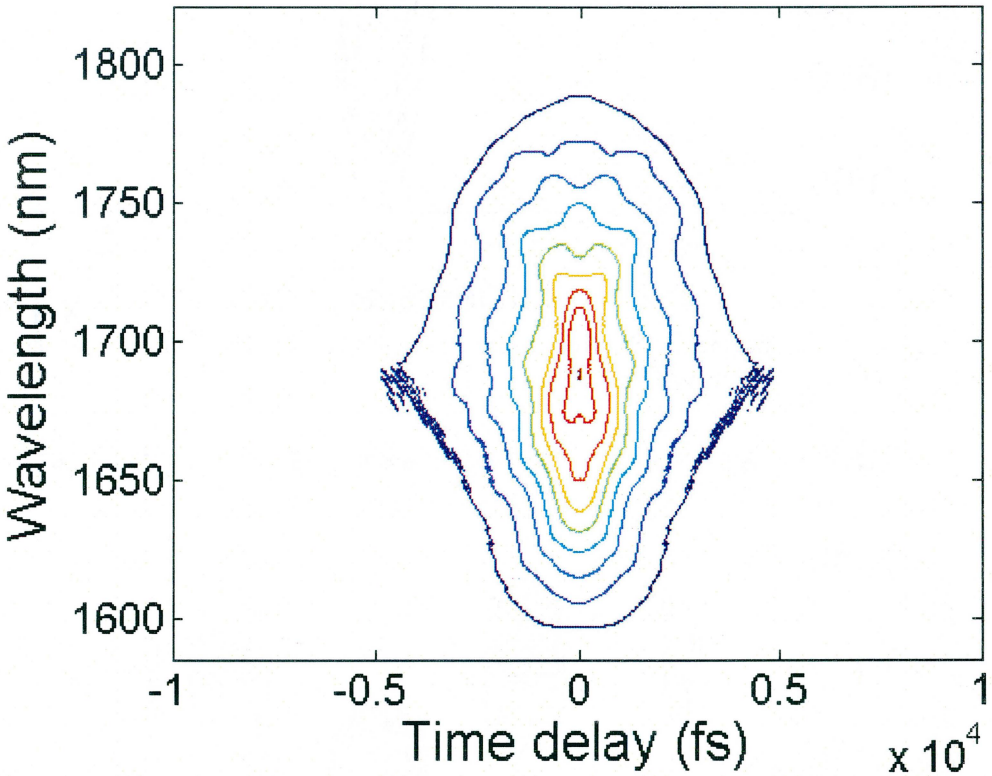

Figure 34. The reconstructed FROG trace after the interpolation of the trace seen in figure 33. The reconstructed part has been zoomed in, in comparison to figure 33.

Due to the instabilities of the laser, the retrieved temporal and spectral FWHM varied from trace to trace. It was only through the retrieval of many different measured FROG traces that a clear picture of the pulse shape could be made. One of the successful retrievals gave the following spectrum and intensity.

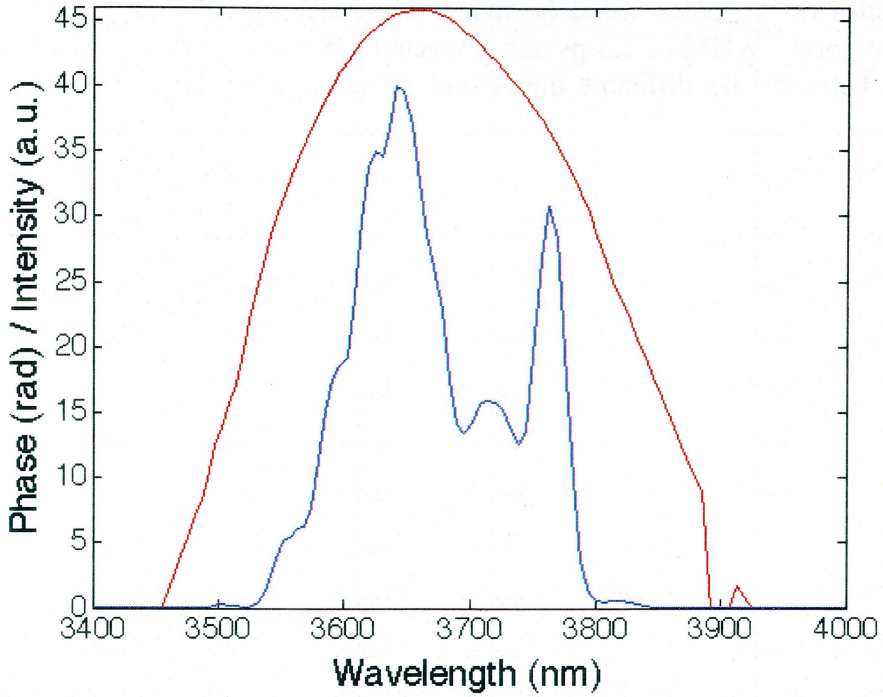

Figure 35. Spectrum, blue line, and phase, red line, of the reconstructed pulse. The GDD of the pulse is clearly visible.

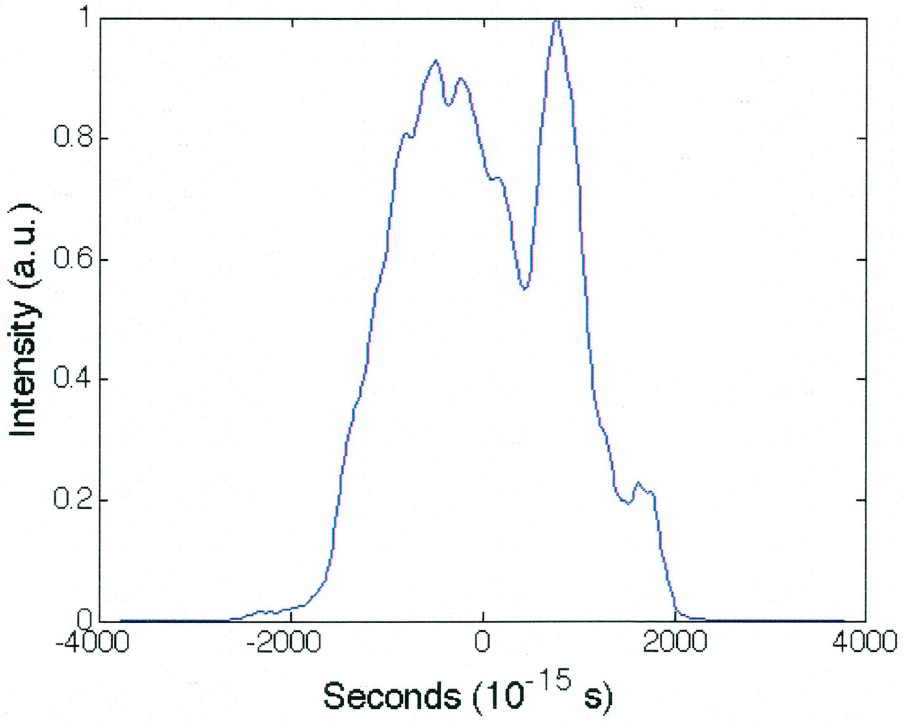

Figure 36. Intensity of the reconstructed trace. Note the similarities with the spectrum in figure 35. This is due to the strong GDD of the pulse.

The large GDD in the pulse led to the similarities in spectrum and intensity as seen in figures 35 and 36. The GDD is strong enough that every single frequency part of the spectrum will arrive at the detector at different times, thus giving the intensity distribution a similar shape as the spectrum.

From many different FROG trace retrievals an estimated average of the characteristics of the pulse could be made. The pulse was determined to have an average temporal FWHM of 2.3 ps and a spectral FWHM of 200 nm. The GDD was consistent between the different traces and an average GDD of 100000 fs^2 was measured.

6 Conclusion

The experimental work of this thesis led to a better understanding of the laser built by Christian Erny. It also produced a FROG setup that is able to measure both temporal and spectral full width half maximum of the laser as well as its group delay dispersion (GDD) and time bandwidth product, i.e. the full pulse shape of the pulse.

The FROG setup was designed to work at two different laser frequencies. One only needs to exchange the beamsplitters and the nonlinear crystals. For the first frequency, the seed of the mid-infrared laser, in short-infrared, 1.07 μm, several FROG traces were recorded. The optimal position of a prism was found to be outside the travel limit of the prism. At the best achieved position of the prism, a GDD of 1000 fs^2 was still present. The FROG traces of the laser show that the laser can radiate in different modes with different temporal FWHM. This is an important conclusion as it makes clear that not only the position of the prism should be optimized, but also the mode in which the laser is radiating should be taken into account to obtain the shortest possible temporal FWHM.

The measurements on the mid-infrared laser, 3.6 μm, were focused on getting a clear picture of the properties of the pulse. An average temporal and spectral full width half maximum of 2.3 ps and 200 nm were retrieved from the scans, which showed a large GDD of 100000 fs^2. The measured spectrum supports pulses down to 90 fs. A new, more broadband stretcher will be installed in the seed laser lowering the possible temporal FWHM even more. The current spectrum (with old stretcher) before amplification supports pulses down to around 30 fs. It is thus plausible that the final temporal FWHM of the compressed pulse will lie in the range 50 to 100 fs.

The values of the mid-infrared laser are an average of the different values obtained while measuring. No exact values could be recreated as the laser was not stable enough. The scans took 30 minutes or more and the laser was normally not stable for more than a few minutes. Thus, the biggest issue arose from the laser being too instable to get a consistent answer. What caused the instabilities? The answer is not entirely clear. Vibrations caused by people being present in the lab room or the lab door being opened caused the power of the laser to jump. Unfortunately, it is not yet clear which parts in the laser that got influenced by the vibrations and caused the jumps. Longtime drifts of the power without anyone being present in the room were also noticed.

6.1 Outlook

The issues caused by the pulse being stretched too much could have been avoided by temporarily recompressing the pulse before measuring it. This mistake was realized too late to be corrected. A first step would be to improve the characterization of the laser pulse. A new spectrometer with a faster scan speed, to minimize the influences of the instabilities of the laser on the measurements, would also be a good investment.

Furthermore, an improvement in laser stabilities is not only crucial for being able to correctly characterize the pulse, but also for conducting later experiments with the laser.

Once fully stabilized and characterized, the laser pulse can be recompressed for use in experiments. One possible technique for recompression would be the use of silicon prism compressors.

7 Acknowledgements

I would like to thank Prof. Dr. Ursula Keller and Dr. Lukas Gallmann for giving me the chance to do my diploma thesis in their group.

A big thank you goes to Anne L'Huillier for giving me the opportunity to go to Zurich.

Thanks to all the great people in the Keller group. Special thanks go to Christian Erny, my supervisor, and the people I shared the office and/or lab with: Dr. Claudio Cirelli, Petrissa Eckle and Adrian Pfeiffer.

Finally I would like to mention Shigeki's sushi party which gave me not only the best sushi I ever tasted, but also one of the best measurements.

8 References

1. L'Huillier, A., et al., *High-order harmonic generation in rare gases*, in *Atoms in Intense Laser Fields*, M. Gavrila, Editor. 1992, Academic Press, Inc. p. 139-206.
2. Tauser, F., F. Adler, and A. Leitenstorfer, *Widely tunable sub-30-fs pulses from a compact erbium-doped-fiber source.* Opt. Lett., 2004. **29**: p. 516.
3. Kane, D.J. and R. Trebino, *Characterization of Arbitrary Femtosecond Pulses Using Frequency-Resolved Optical Gating.* IEEE J. Quantum Electron., 1993. **29**(2): p. 571-578.
4. Iaconis, C. and I.A. Walmsley, *Spectral Phase Interferometry for Direct Electric Field Reconstruction of Ultrashort Optical Pulses.* Opt. Lett., 1998. **23**(10): p. 792-794.
5. Boyd, R.W., *Nonlinear Optics*. 1992, New York: Academic Press.
6. Antoine, P., A. L'Huillier, and M. Lewenstein, *Attosecond pulse trains using high-order harmonics.* Phys. Rev. Lett., 1996. **77**: p. 1234-1237.
7. L'Huillier, A., et al., *High-order harmonic-generation cut-off.* Phys. Rev. A, 1993. **48**: p. R3433-R3436.
8. Dubietis, A., G. Jonusauskas, and A. Piskarskas, *Powerful Femtosecond Pulse Generation by Chirped and Streched Pulse Parametric Amplification in BBO Crystal.* Opt. Communications, 1992. **88**(4-6): p. 437-440.
9. Adler, F., et al., *Phase-locked two-branch erbium-doped fiber laser system for long-term precision measurements of optical frequencies.* Opt. Exp., 2004. **12**: p. 5872.
10. Rodwell, M.J.W., D.M. Bloom, and K.J. Weingarten, *Subpicosecond laser timing stabilization.* IEEE J. Quantum Electron., 1989. **25**: p. 817-827.
11. Eckardt, R.C., et al., *Absolute and Relative Nonlinear Optical Coefficients of KDP, KD*P, BaB,04, Lao3, MgO: Limo3, and KTP Measured by Phase-Matched Second-Harmonic Generatio.* IEEE Journal of Quantum Electronics, 1990. **26**(5): p. 922-933.
12. Rotermund, F. and V. Petrov, *Femtosecond Noncollinear Optical Parametric Amplification in the Mid-Infrared Range with 1.25 μm Pumping.* Jpn. J. Appl. Phys., 2001. **40**(5A): p. 3195-3200.
13. Kato, K., *Second-Harmonic Generation to 2048 A in ß-BaB2O4.* IEEE Journal of Quantum Electronics, 1986. **22**(7): p. 1013-1014.
14. Takaoka, E. and K. Kato, *Thermo-optic dispersion formula for AgGaS2.* Applied Optics, 1999. **39**(21): p. 4577-4580.
15. Trebino, R. and D.J. Kane, *Using phase retrieval to measure the intensity and phase of ultrashort pulses: frequency-resolved optical gating.* J. Opt. Soc. Am. A, 1993. **10**: p. 1101-1111.
16. Gallmann, L., *Generation and Characterization of Few-Femtosecond Optical Pulses*. 2002. p. 53.
17. DeLong, K.W. and R. Trebino, *Improved ultrashort pulse-retrieval algorithm for frequency-resolved optical gating.* J. Opt. Soc. Am. A, 1994. **11**(9): p. 2429-2437.
18. Seifert, B., H. Stolz, and M. Tasche, *Nontrivial ambiguities for blind frequency-resolved optical gating and the problem of uniqueness.* Opt. Soc. Am. B, 2004. **21**(5): p. 1089-1097.

Appendix A: Device Programming

A few of the most used commands for the monochromator and stepper motor can be found in the following two tables.

COMMAND for MONOCHROMATOR	INTERVAL	ACTION
GOTO	0→∞ in 100^{th} nm*	Moves to position
SCAN	0→∞ in 100^{th} nm*	Scans from current position to value
S1ADJ	0→3000 μm	Changes width of entrance slit
S2ADJ	0→3000 μm	Changes width of exit slit
ECHO	Not a Number	Returns ECHO
GRTSEL	1,2,3	Selects a grating
SPEED	0→1200 nm/min	Sets the scan speed

Table A.1. Common commands for the monochromator.[*] There exists no real physical limit of how far one can scan. The resolution of the monochromator is what sets the limit. The further away from the central wavelength you go, the more uncertain the position of each frequency gets.

COMMAND for STEPPER MOTOR	INTERVAL	ACTION
PA	Travel limits of the stepper motor	Moves to an absolute value
PR	Travel limits of the stepper motor	Moves to a value relative to the current position
Speed	100→1.5E6 steps/sec	Sets the movement speed
AC	1.5E4→4.5E8 steps/sec^2	Sets the acceleration

Table A.2. Common commands for the stepper motor.

Example: When ordering the monochromator to scan from 1000 nm to 1300 nm the two following commands were used:

GOTO100000

SCAN130000

The first command will make the monochromator go to 1000 nm and the next command will star the scan.

Appendix B: File Formats

The FROG retrieval program used in this thesis, called simply Frog, was developed by Femtosoft Technologies. When loading a file in the program, one has to give in five parameters, either by hand, or, if present, from the header of the file. The header should contain the following posts: number of delay points; number of wavelength points; delay increment; wavelength increment and central wavelength. With the information in the header and the following spectra, arranged in ascending order relative to the delay point they were measured at, the FROG program automatically reconstructs the measured trace.

Example: The header of a trace with 50 delay points, 320 wavelength points, delay increment 7 fs, wavelength increment 0.3 nm and centered around 1100 nm would look as follows:

50
320
7
0.3
1100

The recorded spectra should follow directly after the header.